We are IntechOpen, the world's leading publisher of Open Access books Built by scientists, for scientists

6,900
Open access books available

186,000
International authors and editors

200M
Downloads

Our authors are among the

154
Countries delivered to

TOP 1%
most cited scientists

12.2%
Contributors from top 500 universities

CLARIVATE ANALYTICS
BOOK CITATION INDEX
INDEXED

WEB OF SCIENCE™

Selection of our books indexed in the Book Citation Index
in Web of Science™ Core Collection (BKCI)

Interested in publishing with us?
Contact book.department@intechopen.com

Supercooling at Melt Growth of Single and Mixed Fluorite Compounds: Criteria of Interface Stability

Jordan T. Mouchovski
Institute of Mineralogy and Crystallography
Bulgarian Academy of Sciences
Bulgaria

1. Introduction

1.1 Single and mixed fluoride crystal compositions – Properties, peculiarities and application

The artificially grown single fluoride crystal compositions of alkali-earth metals (MF_2, $M =$ *Ca, Sr, Ba*) as well as the congruently melted compounds of the type $Ca_{1-x}Sr_xF_2$ or $Ca_{1-y}Ba_yF_2$ possess a high cubic crystal symmetry structure that determines isotropic optical properties of these materials and correspondingly – their broad usability in various optics devices. Amongst the single fluoride, CaF_2 stands out by its unique optical, physical, and mechanical characteristics: light transmission from far ultraviolet (UV) up to middle infrared (MIR), impressive dispersive power and partial dispersion, controllably low stress-induced birefringence, negligible solubility in water and insolubility in many acids, adequate hardness, fairly good thermal conductivity, high resistance to radiation at low luminescence level. The ability of this crystal being a good matrix for rare earth (RE) and actinide completes its superior characteristics and determines exclusively wide application – by variety of optical elements – in UV/MIR and laser optics, holography, dosimetry, lithography, materials processing and other.

Similarly to CaF_2, the matrix of several congruently melted alkali earth (AE) fluoride crystal systems of the type $M_{1-x}M'_xF_2$ ($M \neq M'$) can contain highly concentrated activator RE ions. The physical-chemical properties of such systems, being put under effective control by adjustment of growing conditions, provide production of crystals with desired characteristics. To gain experience in this direction is as much important as the applicability of the mixed AE fluoride compounds expands as: windows in powerful optical quantum generators for laser thermonuclear synthesis, excellent luminescence coverage, Anti-Stokes luminophors, radiation dosimeters, various devices for preservation and optical processing of information and others.

Other mixed systems, formed by congruent melting and crystallization of AE and RE fluorides MF_2–REF_3, represent a high-potential source of new materials in many fields of science and technology. Peculiarity of such systems is that the introduction in the matrix of large proportion of RE ions may result in formation of hetero-valence, strongly non-

stoichiometric solid solutions of the type $M_{1-x}RE_xF_{2+x}$, Here $x \leq 0.5$ and such imposed variations in solid solution composition can be controlled precisely so that to ensure structural micro-homogeneity of the grown crystals with, eventually, some extraordinary physicochemical properties: mechanical (increasing considerably micro-hardness without any cleavage), electrical (amplifying ion conductivity by several orders of magnitude) as well as spectroscopic (strongly improved optical parameters). These type solid solution fluoride crystal systems are used as: structural materials in UV–IR optics; solid electrolytes with high fluorine ion conductivity fast radiation-resistant scintillators, photo-refractive materials, substrates with controlled lattice parameter and low-temperature heat-insulating material; in quantum electronics as host materials and as active elements in solid-state lasers.

1.2 Growing techniques – Interface stability at melt growth

Melt growth of any single or mixed fluoride systems possesses substantial advantages over *growth from solutions* because it may provide conditions for growing homogeneous crystals with two–three orders of magnitude higher crystallization rate (CR). Understandable, the melt growth turned out to be the only method that is appropriate for developing effective techniques for production of crystals with high optical quality (Yushkin, 1983). Specifically, various modifications of Bridgman-Stockbarger (BS) technique are usually employed whereat a container with molten material is moved in vertical two-zone (or multi-zone) furnace, the axial T-gradient of which provides a gradual melt/crystal phase transition (Mouchovski, 2007a). Under thermodynamically grounded segregation effect on liquid/solid interface ($IF_{L/S}$), the distribution of components (impurities) in growing crystal body may become inhomogeneous that causes relevant non-uniformity in its optical characteristics. Nevertheless, in many cases when growing mixed fluoride systems, the residual cationic impurities are of trace concentration so that their impact upon general components' distribution is left negligible.

The growth kinetics itself differs depending on the heat and entropy of melting for particular system, thus determining either face-type (atomically smooth surfaces) or normal (atomically rough surfaces) growth mechanism. As being proved for crystals with fluorite type structure, their heat and entropy of melting turn out sufficiently low for melt growing to proceed by "normal growth" mechanism according to Jackson criterion (Chernov, 1984; Jackson, 2004). In this case the fluoride admixture enriches the crystallization zone (CZ), owing to which $IF_{L/S}$ loses stability in conformity with the degree of so called *constitutional melt supercooling* (CMSc).

2. Melt supercooling as physical-chemical phenomenon

Supercooling phenomenon represents a thermodynamic process of lowering the temperature T of a liquid or gaseous substance below its freezing point T_{fr} without solid phase transition to occur. Below T_{fr} crystallization can start in any liquid (melt) in the presence of either spontaneously arisen nucleus or artificially introduced seed crystal or nucleus. When lacking any such nucleus the liquid may stay down to the temperature whereat homogeneous nucleation to start.

Supercooling arises inevitably when artificial crystals have been grown by BS method, that is, in a container moving downwards in parallel to gravity force temperature field with

negative T-gradient. The phenomenon appears within a very short zone (layer) ahead the crystallization front (CF) as a result of constitutional changes around the moving $IF_{L/S}$ or/and specific heat transport throughout the loaded container (crucible) possessing a complex thermal conductivity. No matter what mechanism results the supercooling, it may affect the smoothness and stability of the CF in micro-level, this way accelerating spontaneous growth of protuberating structures on the $IF_{L/S}$ resulting in growth of crystals with cellular structure.

The nature of CMSc is liable for explanation on the grounds of *conventional crystallization theory* according to which, an extremely fast ionic exchange provides a local quasi-equilibrium on the $IF_{L/S}$. This equilibrium can be disrupted owing to inconformity between the CR and the effective diffusion rates of the ions throughout the supercooled melt zone before their incorporation into the structure of growing crystal. This way the crystal-chemical reactions nearby the $IF_{L/S}$ are diffusion-controlled that is manifested on the phase diagram as difference between liquidus and solidus curves. Under such conditions, the specific change in melt composition ahead the $IF_{L/S}$ causes its geometric and/or morphological instability: the polyhedral crystal form stays unstable, sprouting protrusions at its corners and edges where the degree of supersaturation attains the highest level. The process leads to accelerating spontaneous growth of protruding structures on the $IF_{L/S}$ and growth of crystal with cellular substructure, which is transformed into a dendroid structure.

3. Criteria for interface stability

3.1 Constitutional supercooling principle

For concentrated, two metal component, congruently or incongruently melted, representing mixed fluoride systems of the types $MF_2-M'F_2$ and MF_2-REF_3, the simplest one-dimensional model for $IF_{M/Cr}$-instability considers a normal mechanism in Tiller–Chalmers microscopic approximation (Tiller, 1953), where several factors – the released heat and density jump at crystallization, the contribution of surface energy as well as the anisotropy of segregation coefficient are not taken into consideration. Besides, the low heat of melting for these fluoride systems implies the heat-transport to be neglected at the account of a vast mass transport. Nevertheless when growing large sizes crystals, the mass transport may be concurred strongly by a heat-transport owing to significant radiation flow throughout the growing transparent crystal, surpassing increasingly the conductive flow therein (Deshko et al., 1986, 1990). Disregarding this case, if the thermal field inside the furnace may ensure T-gradient in the melt at the CF, G, that is larger than the gradient of the equilibrium solidification temperature T_L, the derivation of criterion for $IF_{L/S}$-stability starts from the inequality (Kuznetsov & Fedorov, 2008).

$$G = (dT/dz)_{CF} > dT_L/dl \qquad (1)$$

where l is the thickness of the short layer zone ahead the CF.

Further, the material balance at liquid-solid interface is considered relating the CR V_{cryst}, that is, the growing rate, to interdiffusion coefficient (solute diffusivity) D by the equation:

$$V_{cryst}(x_S - x_L) = -D(dx/dl) \qquad (2)$$

Here x_S and x_L are the molar concentrations of solid and liquid phases respectively and *(dx/dl)* – the concentration gradient at the CF.

Eq. (2) unifies the two types mass transport, the jump-like forcing-out (when the equilibrium coefficient of segregation k_o < 1) and absorption of the second component and its diffusion into the melt bulk or from the bulk (when k_o > 1).

Using the mathematical expression:

$$dT_L / dl = (dT_L / dx)(dx/dl) = m(dx/dl) \qquad (3)$$

where the slope *m* of the liquidus curve (tangent of the slope's angle for the liquidus curve) is being introduced, from (1) and (2) it follows:

$$G\, D/V_{cryst} > m\, \Delta x \qquad (4)$$

Here $\Delta x = x_S - x_L$ expresses the apparent discontinuity in component's concentration at the CF.

The inequality (4) is an extension to region of the high concentrations and non-stationary processes of Tiller–Chalmers stability criterion (Chalmers, 1968):

$$G/V_{cryst} > -\, m(1 - k_o)x_{o(b)}/k_o\, D \qquad (5)$$

where: $x_{o(b)}$ is the admixture molar concentration of the second (impurity) component in the melt prior to solidification, equal to its mean concentration in the melt bulk (sufficiently far from the CF), while k_o is defined by the ratio of solid x_{oS} to liquid x_{oL} phase concentrations for this component, specified at the CF.

This criterion, derived under suggestions of stationary crystallization caused by CMSc, small concentration for the second component and constant values for k_o and *m*, has been proved being valid for concentrated melts as well (Kaminskii et al., 2008; Sobolev et al., 2003).

The solution of the van't Hoff equation:

$$dlnk_o/dT = L_{molt}/RT^2 \qquad (6)$$

for the case of coexisting phases in binary systems with low content of the second component gives the expression:

$$m = \Delta T/\Delta x_o = (RT^2/L_{molt})(k_o - 1) \qquad (7)$$

where *R* is the universal gas constant and L_{molt} is the enthalpy of melting (latent heat of fusion) for matrix material (the first component).

The application of later equation makes it possible to determine *m* from the liquidus curve at $x \to 0$ (initial slope of the curve, m_{init}) and, correspondingly, k_{olim} – the limiting segregation coefficient of the admixture when its concentration tends to zero. Thence:

$$k_{olim} = (L_{molt}/RT^2)m_{init} + 1 \qquad (8)$$

Substituting (7) for *m* in (5) the criterion for interface stability takes the form:

$$G\ D/V_{cryst} > - (RT^2/L_{molt})(k_o - 1)(1 - k_o)x_{o(b)}/k_o = (RT^2/L_{molt})x_{o(b)}(1 - k_o)^2/k_o \qquad (9)$$

which, in case of slightly soluble into the lattice impurities ($k_o << 1$), can be approximate by:

$$G\ D/V_{cryst} > (RT^2/L_{molt})x_{o(b)}[(1/k_o) - 1] \qquad (10)$$

The physical explanation of criterion (10) is grounded on so called *segregation mechanism*, under which impact are all kind of impurities penetrated in trace concentrations within the layer ahead the moving CF. These impurities are usually several metal cations and oxygen containing anions, any concentration gradients of which arisen can not be equalized at a lack of sufficiently intensive convection into the melt bulk and relatively low diffusion rates. Hence, kinetic limitations determine the real crystallization conditions liable for impurities' segregation at the CF. Mathematical this phenomenon is convenient being expressed by introducing in (5) an extra multiplayer, k_{eff}, the so called effective coefficient of segregation (Sekerka, 1968):

$$G/V_{cryst} > - (m\ x_o/D)[(1 - k_o)/k_o.]k_{eff} \qquad (11)$$

Here:

$$k_{eff} = k_o/[k_o. + (1 - k_o)exp(-\Delta)] \qquad (12)$$

where the index $\Delta = V_{cryst}\ \delta/D$ has a meaning of "*reduced CR*" and δ is the thickness of the diffusion boundary layer.

Evidently the parameter Δ decreases with lowering V_{cryst} or δ and with an increase of D whereat the denominator in (12) enhances, tending to 1 at $\Delta \rightarrow 0$. Correspondingly k_{eff} goes down, tending to the equilibrium segregation coefficient k_o. The other limiting case ($\Delta \rightarrow \infty$) leads to $k_o \rightarrow 1$, that is, the impurity's content in the crystal stays equal to that in the melt bulk.

The position of k_{eff} as regards k_o depends on whether the equilibrium coefficient stays lower or higher than unity: if $k_o > 1$, then the inequalities $1 < k_{eff} < k_o$ are being fulfilled. Opposite to that, if $k_o < 1$ (as in the cases for mostly RE in fluorite matrix (Nassau, 1961), then $k_o < k_{eff} < 1$.

The thickness of the diffusion boundary layer δ, assessed approximately of the order of 0.1 cm, can be substantially reduced in case of stirring the melt whereat it approaches a limiting value of 0.001 cm, conditioned by liquid to solid adhesion. Thus, providing sufficiently intensive stirring of the melt, one may anticipate considerable enhancement of $IF_{L/S}$-stability. Without such stirring, owing to low diffusion rate in liquid phase for the heterogeneous impurities, they either enrich (at $k_{eff} < 1$) or impoverish (at $k_{eff} > 1$) the layer ahead the $IF_{L/S}$. This way attained enhancement/lowering of impurities' concentration causes a relevant local lowering of melt temperature in the layer, followed by rejection of the impurities from crystallizing surface and their embedment in crystal lattice. At that the equilibrium freezing temperature in the melt adjacent to CF remains above the real temperature established. As a consequence, numbers of nucleolus centres appear simultaneously in supercooled layer that breaks the morphological $IF_{L/S}$ stability. In conformity with that the normal growth turns out replaced by high rate poly-crystalline (dendroidal) solidification with formation of cellular sub-structure. Such trapped impurities appear as well light-scattering centres lowering the light transmission within corresponding spectral range.

The approximation (10), giving deviation below 1% for $k_o \leq 0.01$, is especially convenient to demonstrate clearly how it could be attained specific conditions, guaranteeing the interface stability, varying appropriately definite substantial and/or apparatus factors so that the influence of the second (impurity) component to be neglected.

3.2 Function of stability and interdiffusion coefficient

The right-hand side of inequality (4) is denoted by $F(x)$ as function of stability (P.I. Fedorov & P.P. Fedorov, 1982; Turkina et al, 1986; Van-der-Vaal's & Konstamm, 1936), possessing dimensionality of temperature. The function is nonnegative $F(x) \geq 0$, vanishing at points with pure components and at the extremes (points of congruent melting of the solid solutions) where the liquidus and solidus have gotten tangential points. In the range of small impurity's concentrations $F(x)$ approximates a straight line (Djurinskij & Bandurkin, 1979). To a first approximation $F(x)$ can be expressed by the T-difference between liquidus and solidus curves.

The function of stability reveals definite physical meaning as regards the real crystallization process: there is no concentration supercooling and the CF should keep a planar and stable form for any cases when the value of parametric combination $G D/V_{cryst}$ lies higher at a given x_s than the corresponding point pertaining to $F(x)$-curve. In this combination the furnace design and power supply distribution are decisive for determining the steepness for G. After establishment of this gradient, V_{cryst} is under control either by altering the speed of crucible (SC) withdrawal or by cooling slowly the immobile load by Stober growing technique so that both cases the growth to proceed within constitutional regions of interface stability. Such approach requires an eventual compositional dependence for interdiffusion coefficient D to be searched by using an expression, following from (4):

$$D = m \, \Delta x (V_{cryst}/G) = F(x)_{crit}(V_{cryst}/G) \qquad (13)$$

where $F(x)_{crit}$ is the critical stability function upon the transition from stable plane CF to unstable one, the values of which function are calculated with sufficient precision from corresponding compositional phase diagram for particular fluoride system. Here special attention should be paid to number of points, for which dataset precision is *in situ* high: the melting temperatures for the end members of studied solid solution, the extremes (maximums or minimums) on the melting curve, and eutectic equilibriums.

3.3 Perturbation theory of interface stability

The inequalities (5), respectively (9), appear appropriate criterion for quantitative analysis about the influence of any impurities on melt supercooling arising ahead the CF in accordance with their amount and solubility into the structure of growing crystal. Processing the experimental data on hand, concerning $IF_{L/S}$ stability of many single crystal compositions and metal alloys, Sekerka (1968) outlined mostly of them being in satisfactory agreement with inequalities (5) or (9). However abiding this criterion, based on purely thermodynamic considerations, failed in several other cases due to its shortcomings. Indeed, the constitutional supercooling principle refers only to liquid phase, thus ignoring the latent heat of fusion and the heat flow throughout the growing crystal. Unlike it, the *perturbation theory of interface stability* has been developed being based upon the dynamics of the whole melt-crystal system (Mullins & Sekerka, 1963, 1964; Sekerka, 1965, 1967, as cited in Sekerka,

1968). Besides, this theory provides a description of time evolution of the perturbed interface, following the alterations in thermal and concentration fields. It seams this theory should replace that of CMSc principle despite giving a much more complicated expression for perturbation $IF_{L/S}$ stability criterion (Sekerka, 1965). One may assess the reasonability of such replacement after writing the perturbation $IF_{L/S}$ stability criterion in a form usable for comparative analysis to inequality (5):

$$(G/V_{cryst}) + (L_{molt}/2K_L) > [-m(1 - k_o)x_{o(b)}/k_o D][(K_S + K_L)/2K_L] \varphi \tag{14}$$

Here, the latent heat of fusion L_{molt} refers to unit volume of the solid crystal phase; K_L and K_S present the thermal conductivities of the liquid and solid phase, respectively; φ is function of stability that depends in a complex way on k_o, m, $x_{o(b)}$, D, V_{cryst}, the absolute melting point of the pure solvent (first component), and Γ-function, that expresses melt-crystal surface free energy.

Since $\Gamma \leq 0.001$, φ is usually between 0.8 and 0.9, approaching 1 for negligibly small surface free energy. Such relatively small deviations of φ from unity illustrate a tendency of the surface free energy to stabilize slightly the $IF_{L/S}$. Here some comments are useful: the divergence between the results, obtained by criterions (5) and (14), becomes greatest for small concentrations, $x_{o(b)}$, of the second (impurities') component. Thence, for the first, highly concentrated component (the matrix), it exists a certain limiting concentration for the second component below which, even at very fast crystallization rates, a cellular structure could not be formed so that the established planar CF would be absolutely stable. Nevertheless, with increasing the concentration of the second component, the contribution of the surface energy lessens rapidly and may be neglected. It should be notice as well that it is possible the corrections due to surface energy stabilizing effect to become significant around the extreme points upon the melting curve for several mixed fluoride solid solutions.

The ratio $[(K_S + K_L)/2K_L]$ in (14) may affect tangibly the $IF_{L/S}$-stability only if K_S is appreciably higher than K_L. Opposite to that, when thermal conductivities of the two phases are close to each other, this factor stays insignificant for assisting the criterion (14) being fulfilled. However in case the growing medium is optically transparent (as appear mostly single and/or mixed fluoride compounds), not conductivity but radiation should determine the heat transport throughout the load. Besides, the melts of these compounds turn out semi-transparent. Despite the thermal processes for such liquid-solid systems have been described by a system of integral-differential equations solved at specific boundary conditions, the developed on this grounds non-linier stability theory leads inevitably to considerable mathematical complications and difficulties for correct interpretation of the results. Both later could be overcome by using a simple model where thermal conductivities were replaced by their effective analogs, representing a sum of thermal and radiative conductivities for corresponding phases (Mouchovski, 2006). This model has been checked being a good approximation in case of CaF_2 single crystal growth at usually imposed BS thermal conditions (Mouchovski, 2007a) where the effective conductivities for both phases were estimated being approximately 20 times higher than their constituting thermal conductivities.

Analyzing further the inequality (14) it is seen the second term on its left-hand side, $(L_{molt}/2K_L)$, should have stabilizing effect upon interface stability; this effect is as much

pronounced as the latent heat of fusion is larger and/or the thermal conductivity of the melt is lower. For crystals with semi-transparent melts where $K_{Leff} \approx K_{Lrad} >> K_{Lconc}$ the real contribution of $(L_{molt}/2K_{Leff})$ should be relevantly small.

3.4 Normal growth criterion

Any analysis of supercooling effect, causing transition from mono-crystalline to cellular growth for solid solutions with fluorite structure, will be correct only if normal growth proceeds on a rough surface. It is considered this mechanism being involved when the value of normalized latent heat of fusion $L_{molt}/kT_{m.p.}$ (k – is the Boltzmann constant and $T_{m.p.}$ – the m.p. absolute temperature) stays below 2 (Jackson, 1958) or below 3.5 (Alfintzev et al., 1980). As shown in case this criterion failed, the growth proceeds by formation of two-dimensional nucleation. At that the high anisotropy of the process prerequisites both, the segregation coefficient and the surface energy for considered impurity, to depend strongly on growth direction. In this case besides cells' formation, a laminar distribution of impurity can occur caused by capturing of melt's layer adjacent to the growth surface.

4. Function of stability and properties for mixed fluoride systems

4.1 Mixed alkali earth fluoride systems

The alkali earth metal single fluorides MF_2 may form tri- or four-component solid solutions of type $Ca_{1-x}Sr_xF_2$, $Ca_{1-y}Ba_yF_2$ or $Ca_{1-x-y}Ba_xSr_yF_2$, which retain the cubic symmetry of the fluorite lattice. However, complete solubility of the starting single fluorides has proved to be possible only for the first system, the compositional phase diagram of which manifests a clear minimum for $0.4 < x < 0.5$ (Chern'evskaya & Anan'eva, 1966; Klimm et al., 2008; Weller, 1965) while the system's properties appear intermediate between those of CaF_2 and SrF_2 end members. Correspondingly the compositional dependence for stability function starts from and ends to zero K, being insignificant at the extreme minimum (Klimm et al., 2008). This crystal system has been recently an object of thorough investigation within a large compositional interval for specific case of simultaneous growth of batch of parallel boules with different x where for CaF_2 was utilized fluorspar, concentrated to above 99.6 wt.% (Mouchovski, 2007b; Mouchovski et al., 2009a, b; Mouchovski, 2011).

Completely different behaviour at room temperature possesses CaF_2–BaF_2 system owing to a large difference in ionic radius between Ca^{2+} and Ba^{2+} and, accordingly, in lattice parameter between CaF_2 and BaF_2. As a result, after a primary crystallization of a continuous series of $Ba_{1-x}Ca_xF_2$ fluorite solid solutions with a minimum in the liquidus curve at $x < 0.5$, during the cooling there occurs a high-T (at 900 °C) solid-state decomposition into a two-phase mixture of dilute CaF_2 and BaF_2-based solid solutions (Chernevskaya, & Anan'eva, 1966; Wrubel et al., 2006; Zhigarnovskii & Ippolitov, 1969). The phase diagram of this system has been recently reviewed by Fedorov et al. (2005) who showed it does not contain a continuous solid solution. Thus, on cooling the 70CaF_2–30BaF_2 melt (mol%), a $Ca_{1-y}Ba_yF_2$ solid solution (*a*-phase) solidifies as a primary phase, which at (1039 ± 5) °C reacts with the melt to form a second fluorite α-phase, $Ba_{1-x}Ca_xF_2$. This *a*-solid solution decomposes on further lowering the temperature into two phases: a_1 and a_2. When the temperature reaches (870 ± 5) °C, it comes up to a eutectoid equilibrium between three fluorite phases: a_1, a_2, and β. This equilibrium is broken at lower temperature since quenching at a rate of 250 °C/s cannot

retain the a_2-phase and it is decomposed. As a consequence of these thermal events, the resultant composite material consists at room temperature of two fluorite phases, a_1 and β. Surprisingly, it posses a unique ionic conductivity that is respectively 25 and 330 times higher than those of the parent BaF_2 and CaF_2 – phenomenon that was explained in terms of the electrical properties of the material's interfaces (Maier, 1995). Materials with such properties appear of great interest for solid-state ionic opening up new opportunities for engineering medium temperature fluoride ion conductors (Sorokin et al., 2008).

Nevertheless, the mixed AEM fluoride crystals have been studied mostly for their promising lasing properties after doping/co-doping by appropriate trivalent Ln-ions with eventual charge-compensation by univalent alkali ions. For Ln^{3+}-based lasers these properties depend strongly on both the symmetry and strength of the crystal field so they may be purposely controlled by appropriate modification of the host material.

4.2 Mixed alkali earth – Rare earth fluoride systems

As denoted by Fedovov at al. (1988) the phase diagram and resulting function of stability for any MF_2–REF_3 system is in accordance with the type and sizes of RE ionic radius that, in turn, reflects on relevant interdiffusion coefficient. The authors established a regular dependence of $F(x)_{crit}$ on RE ionic radius, with a clear minimum for M = Ba and Sr, corresponding to transition from $k_o > 1$ for the larger cations in the beginning of the Ln-series to $k_o < 1$ for the smaller cations pertaining to the yttrium sub-series. In case of M = Ca any regularity was not found due, probably, to fine partitioning of the Ln-series on several sub-series (Djurinskij & Bandurkin, 1979). Further calculations led the authors to interdiffusion coefficient for La (the RE with largest ionic radius), D_{La} into fluorite matrix being independent on partition of LaF_3 second component when its concentration exceeded 0.16 mol.%. At the same time D_{RE} was shown to keep a linear dependence on RE-radius, decreasing approximately twice from La to Yb in the range of 10^{-5} cm^2/s.

Extending broadly the investigation of MF_2–REF_3 systems, Kuznetzov and Fedorov (2008) established empirically a clear maximum in solidus compositional dependence of k_o for SrF_2–CeF_3 system, expressing it by power function equation, the coefficients of which appear complex functions on data extreme. The relevant $F(x)_{crit}$, showing a slight maximum (10 K) at $x_S = 0.1$ mol.% and nearly zero minimum at $x_S = 0.25$, goes up hyperbolically attaining so high values at $x_S > 0.5$ that excluded, in practical the formation of solid solution crystals. The same specificity for $F(x)_{crit}$ dependence on x_S were found out for Nd, Pr and La whereas for the rest REs the authors did not reported of any maximum at low RE content. They announced similar results in case M = Ca where $F(x)_{crit}$ started to increase hyperbolically without any intermediate maximum, being less pronounced for Ce whereas for La $F(x)_{crit}$ tended to linearity as for $x_S < 0.5$ its values stayed firmly below 25 K. In case M = Ba, again for Ce, Nd, Pr and La it was established the specific for M = Ca maximum – minimum – hyperbolical increasing succession of $F(x)_{crit}$ dependence where the maximum variations were larger when being displaced towards the lower x_S. For the rest RE significant alterations in curves' course were obtained that suggests formation of variety of complex structures consisting in large Ba ions and much smaller, different in sizes RE ions. To the same suggestion leads the comparison of $F(x)_{crit}$ vs. RE radius dependence for Ca and Ba respectively; one can see a clear minimum for M = Ca, displaced to larger radiuses for higher concentrations whereas the minimum turns out considerably broadened when M =

Ba. Accordingly to these results one may anticipate specific behavior of the key physical-chemical properties for studied mixed fluoride systems grounded on their structural peculiarities. Here of particular importance appears the thermal conductivity T-dependence mostly used for assessing the eventual application of particular MF_2–REF_3 systems for creation of highly effective solid-state lasers, with RE^{3+} as activator.

Nowadays it is apprehended $M_{1-x}Yb_xF_{2+x}$ systems with $x < 0.5$ being with priority as comparing corresponding $M_{1-x}Nd_xF_{2+x}$ systems since the usage of Yb^{3+} instead Nd^{3+} as ion-activator in laser materials leads to several approved advantages: *i*) simplicity of the structures of the laser levels for ytterbium; *ii*) smaller difference between the wavelength of pumping and generation of pulses; *iii*) lowered heat losses; *iv*) wider bands of the emission spectrum that is especially convenient for generation of short pulses and creation of tunable lasers with larger lifetime of the upper excited level. Here again the usage of CaF_2 for the matrix seams most promising and combination CaF_2–YbF_3 leads to formation of heterovalent fluoride solid solution $Ca_{1-x}Yb_xF_{2+x}$ at $x \leq 0.41$ (Ito et al., 2004; Lucca et al., 2004; Sobolev, & Fedorov, 1978). The thermal conductivity T-dependence for this system has been investigated thoroughly by Popov and co-workers (2008a) that established specific alteration in conjunction with considered compositional interval. At the lowest compositions, $x \leq 0.001$, a decrease of thermal conductivity with increasing T was observed within 50-300 K, that is, up to room temperature. Such behavior is typical for crystalline materials and corresponds to a decrease in the mean free path of phonons with temperature. For x within 0.005–0.03, smooth maximums were noted in the curves that turned out displaced downward into the range of high T with increasing x. Importantly, in the low T-interval there occurs a transition from behavior typical of single crystals (with a maximum in T-dependence) to behavior characteristic for glasses, with a monotonic decrease in thermal conductivity with T-decrease. As firmly considered such transition to glasslike structures is connected with formation, accumulation, and agglomeration of clusters of oppositely charged defects, which leads to disturbance of short-range order with retention of long-range order [Fedorov, 1991, 2000; Kazanskii et al., 2005; Sobolev et al., 2003). Within the next compositional interval, $x = 0.09$–0.25, the thermal conductivity, was found out to grow up monotonically with T, which is typical behavior for any disordered systems but is completely inadmissible for crystals of simple stoichiometric compounds. Similar glasslike behavior of any concentrated heterovalent solid solutions $M_{1-x}RE_xF_{2+x}$ of REF_3 into fluorite-type compounds MF_2 (M = Ca, Sr, Ba, Cd, Pb) was noted repeatedly (Fedorov, 2000) for the thermal conductivity as well (Popov et al., 2008b, c). Here unifying result appeared the mean free path for phonons (within 0.09–0.25 compositional interval) was found only weakly T-dependent, becoming on the order of unit-cell dimensions (Popov et al., 2006). This fact suggests "growth-in" of clusters into the fluorite-type lattice and appearance of nanoheterogeneity in the relevant solid solutions.

5. Purpose and aims: Control upon interface stability and crystal quality

It can be distinguished two types of factors, influencing the stability of growing interface: substantial factors that refer to peculiarities of growing compounds, determining liquidus–solidus phase diagram, and technological (apparatus) factors related to configuration of the thermal field, established into the load, and the real CR. Nevertheless the technological factors are in subordinated position to the substantial ones since the proportion of starting

compounds predetermines often the region of permissible alterations for the imposed thermal conditions and the speed of crucible withdrawal.

The present survey deals with different approaches for providing an efficient control upon morphological and geometric stability of the moving CF, keeping its shape near to planar during the growth of particular single or mixed fluoride systems. The accent is being put on single CaF_2 and $Ca_{1-x}Sr_xF_2$, where both cases natural fluorite (fluorspar) is being used as starting material. The influence of several different impurities (eutectic particles of non-soluble compositions) or ionized molecules (oxygen-containing anions or cations embedded into the lattice) upon interface stability is analyzed semi-quantitatively for single CaF_2 by using simple supercooling criterion. Here the aim is how to be implemented an efficient control on trace levels of residual impurities into starting fluorspar and its melt as well as on other contaminants that enter eventually the CZ during crystallization itself.

The same supercooling criterion is being utilized for investigating the stability function in case of simultaneously growth of $Ca_{1-x}Sr_xF_2$ boules with different composition. Here the exact knowledge of liquidus–solidus phase diagram is rather important in particular, when for CaF_2 end member is being chosen two types fluorspar, differing each other with RE impurities' content (total amount below 100 ppm). Thus specified phase diagram (with expected decrease of the initial negative slope and displacement of the minimum towards the lower Sr-content x (Mouchovski, 2007a) should alter relevantly the effective segregation coefficient, which equilibrium value appears a structurally sensitive characteristic of the mixing processes. Here aim is determination of the compositional dependence for k_o that will offer scope for hypothesizing about possible mechanisms for incorporation of the second component – Sr ions with CaF_2 matrix (first component).

The phase diagram character influences decisively as well the interdiffusion coefficient, so that the determination of its compositional dependence is another aim of the study.

The optical characteristics of thus grown crystals – as most sensitive properties of the medium – are measured, aimed they being related to corresponding values for stability function for comparative analysis to be implemented.

As general goal of the survey appears determination of appropriate interval for crucible speed towards the cold furnace zone, within which a normal growth to proceed at minimal supercooling effect in conjunction with the established real temperature distribution into the load. This means to be implemented control upon the technological factors so that: i) to be attained controllably sufficiently steep axial (vertical) T-gradient into the furnace unit (FU), keeping at that a minimal radial T-gradient into the load whereat a planar or slightly convex $IF_{L/S}$ to be maintained; ii) to be set up an appropriate SC, that to be very close to the real CR along the mostly crystal length.

6. Methodology

Complex growing methodology is applied to provide minimum contamination into CZ, and effective control on the thermal condition into the FU.

It is implemented efficient deep preliminary purification (PP) of the starting fluorspar for substantial reduction of mostly metal cations (except those pertaining to Ln-group) and some metal oxides resulted from decomposition of accessory minerals accompanying the

basic fluorite. The PP includes consecutive chemical treatment of grained fluorspar portions into HCl and HF acids followed by high-T treatment in the presence of melt scavenger (up to 2 wt.% PbF_2 or/and ZnF_2 additives) so that the purity of the produced polycrystalline/sintered precursors attains level of 99.6 wt.% (Mouchovski et al., 1999; Mouchovski, 2007a).

Crystal growth by BS technique, where the constant speed of crucible withdrawal is step-wise changed between 0.2 and 0.6 cm per hour, is accomplished into two types' multicameral crucibles, the specific construction of which assist for restricting considerably penetration into CZ of undesired oxygen/water vapour ionised molecule from the vacuum chamber environment. Specifically, the sizes of the openings (channels) into inner cameras' lids are adjusted of order of the mean free path of gaseous ions so that their back movement inside the cameras being under control by Knudsen diffusion (Mouchovski, 2007a).

Both types' multicameral crucibles consist of central nest surrounded by several axi-symmetric peripheral cameras (Mouchovski et al., 1996). The first type crucible ("Tube support") contains 9 cameras-inserts (with diameter of 2.48 cm), placed in parallel and close to each other in peripheral tubular compartment. The free spaces around and above the inserts are, essentially, additional mass-transport resistance as regards all gaseous species penetrating from vacuum environment. Opposite to that, the 8 cameras (with diameter of 2.56 cm) of the other type crucible ("Revolver support") are surrounded my solid graphite mass, the relatively large thermal conductivity of which ensures the radial heat flux throughout the load (graphite walls surrounding crystallizing molten portions of fluorspar and several connected free spaces) being correspondingly released.

The thermal field in such complex load follows the set T-programs for furnace power supply of tailor-made Bridgman-Stockbarger Growth System (BSGS). Its FU consists of close package graphite screens wherein upper and lower heaters differentiate hot (Z1) and cold (Z2) zones, respectively, separated by diaphragm (SD), differentiating relatively long adiabatic zone (AdZ) wherein the radial heat-exchange should expect being insignificant. Supplementary, system of molybdenum shields, part of which is related to moving crucible, has been introduced into the FU. The altering configuration of this system allows much more precise regulation of the thermal field into the FU and into the load, respectively (Mouchovski, 2007a). The details are discussed in sub-section 7.2.

Products of crystal growth are batch of simultaneously grown boules wherefrom are prepared pairs of parallel optical windows, taken from one and the same sections of the cylindrical body of the boules. The windows are finished according to requirements for laser grade CaF_2 (Mouchovski et al., 2011) that reduces considerably the reflectivity radiation losses from the parallel planes surfaces within and below UV region. Approximately equal distance (0.6–1 cm) between windows' pairs for each particular batch of boules allows implementation of reliable comparative analysis of composition and characteristics of the grown crystals.

The windows are utilized for determination of: *i*) Ca-proportion, (1-*x*), in the final solid solutions by using of X-ray diffractionless analyzer BARS-3; *ii*) light transmission *t*-spectra, measured within UV-IR range by means of high-sensitive spectrophotometer, a Varian Cary type 100. Series of *t*-measurements are also obtained at discrete wavelengths ($\lambda = 248.3$ nm, 510.6 nm and 6.45 µm) by applying so called Valour Lasers Irradiation technique (VLIr)

(Mouchovski et al., 2011). The corresponding light extinction losses per unit optical path are calculated from formulas grounded on Lambert-Beer law approximation where t is presented as a sum of absorption and scattering parts and window's plane surface reflectivity is being excluded.

The stress-induced birefringence in the windows is determined by means of polariscope/polarimeter PKS-250.

The concentration and distribution of residual impurities along the height of grown boules is determined applying Atomic Absorption Spectroscopy (AAS), Solid Sampling Electrothermal Atomic Absorption Spectrometry (SS-ETAAS) and Neutron Activation Analysis (NAA) – for the RE elements – techniques (Detcheva & Hassler, 2001; Detcheva & Havezov, 1994, 2001, 2005, as cited in Mouchovski, 2007).

For assessing the CF position, x_{CF}, along the FU it is applied originally developed indirect technique, which involved determination of a Quenched Interface (QI) in multicameral crucible loaded by portions of concentrated grained fluorspar (Mouchovski et al., 1996a).

Empirically derived formulas, given elsewhere (Mouchovski, 2007a), relate x_{CF} to x_1-variable (expressing crucible movement from the starting position) and the changes in the set T-regimes of furnace heaters. The origin of the basic axial coordinate, z, lies on FU cross-section separating AdZ from Z2. The height of crystallizing part of the boules is determined by the difference ($x_{CF} - x_{con}$) where x_{con} defines the distance passed by the plane section of the conical cameras' tips. All variables are reduced appropriately to take dimensionless form. The boules' height h_{boule} is expressed in x_1* units as partition from crucible withdrawal for a given run by formulas:

$$x_1* = (z_{incon} - z)/l_{crmov} \tag{15}$$

and correspondingly:

$$z = z_{incon} - l_{crmov} \times x_1* \tag{16}$$

where z_{incon} is the initial position of cameras' tips wherefrom the crystallization begins to propagate at the chosen starting position of the crucible into Z1 and l_{crmov} represents the distance whereto the crucible moves downward into the FU.

The real T-gradient along the FU is assessed approximating the calculated axial T-gradient obtained after differentiating the axial T-profile of the furnace, measured in empty crucible (Mouchovski et al., 1996).

The real CR is estimated as the set SC is being corrected accordingly the varying shift in $IF_{L/S}$ position during crucible movement.

The liquidus – solidus curves for particularly studied $Ca_{1-x}Sr_xF_2$ system (Bulgarian fluorspar as starting material) are obtained by DTA measurements accomplished using a Stenton Red Croft STA instrument in argon flow and using graphite crucibles. The measured points lie within the experimental error on curves estimated by using formula, adopting recently specified phase diagram for the system in case both end members are chemical compounds [see Fig. 3 in Mouchovski et al., 2011]:

$$T_{liq/sol}(Mouh) = T_{liq/sol}(Klimm) - (1-x)\,\Delta T_{x=0} \tag{17}$$

Here a linear decrease is being approximated for calcium proportion $(1-x)$ with the initial CaF_2 m.p-difference, $\Delta T_{x=0}$, equal to $1691 - 1648 = 43$ K for the used types of fluorspar.

Thus obtained datasets are fitted by 8-order polynomial with correlation coefficient above 0.99.

The critical values for stability function $F(x)_{crit}$ are calculated from the phase diagram where both dependences, $m(x_o)$ and $\Delta x_o = x_S - s_L$ are indirect functions of T.

The compositional dependences of segregation coefficient and interdiffusion coefficient are calculated from (8) and (13) being in conjunction with found alterations of the real T-gradient and real CR during the growth of each particular boule.

7. Experimental

7.1 Interface stability during the growth of CaF$_2$ crystals

Effect of oxygen-containing contaminants on interface stability

In case of CaF_2 crystal growth by using fluorspar, the melt of which is contaminated by oxygen-containing molecules/ions, a sequence of physical processes and chemical reactions leads to eutectics formation since the produced final compound – CaO – is not isomorphic with CaF_2 and cannot dissolve into the lattice to form a solid crystal solution.

The eutectics formation may consider on the grounds on supercooling effect arisen. For the purpose the right-hand side of criterion (10) is presented by the crucial T-gradient along the layer ahead the CF with thickness δ_i, whereat the equilibrium between the average interdiffusion coefficient for particular impurity "i", D_i, and the maximum linear CR, V_{cryst}, starts to disrupt:

$$\Delta T_{cru}/\delta_i = (RT_{cr}^2/L_{molt})[x_{o(b)}(k_{eff}^{-1} - 1)](V_{cryst}/D_i) \tag{18}$$

Substituting the proportion between the average diffusion coefficient, D_i, and V_{cryst} for δ_i in (18), the decrease in crystallization temperature T_{crys}, due to enrichment of the layer ahead the CF by particular impurity, is expressed by ΔT_{crys}-quantity according to formula:

$$\Delta T_{cru} = (RT_{cryst}^2/L_{molt})[x_{o(b)}(k_{eff}^{-1} - 1)] \tag{19}$$

In case CaF_2 crystal growth proceeds where the used fluorspar possesses m.p. (1648 ± 5) K and $L_{molt} = 7100$ cal/mole, then $(RT_{cryst}^2/L_{molt}) = (760 \pm 2)$ K. Thus, when the principal contaminant is insoluble CaO with $k_{eff} \ll 1$, it is fulfilled $(k_{eff}^{-1} - 1) \gg 1$. At this junction even at relatively small CaO concentration, the product $[x_{o(b)}(k_{eff}^{-1} - 1)]$ may attain significant value, exceeding of two order of magnitude $x_{o(b)}$. Using arbitrary: $k_{eff} \approx 0.01$ and $x_{o(b)} = 5 \times 10^{-4}$ mole parts, the calculated T-fall is significant: $\Delta T_{crys} \approx 39$ K.

On the other hand, D_i for O^{2-} dissolved in CaF_2 melt is too low ($\approx 10^{-11}$ m^2/s) so that these anions are immobile in practical compared to F^- anions, which, possessing nearly the same effective ionic radius, bear twice less negative electrical charge. At this junction, within the usually attained interval for V_{cryst} that follows approximately the SC (2–10 mm/h), δ_i stays of order of 10^{-3} cm (10 μm) while the crucial T-gradient, $\Delta T_{cru}/\rho_{im}$, is calculated equal to 3.9×10^4 K/cm (39 K/μm). Such extremely steep positive T-gradient along the enriched to CaO layer

ahead the CF should exclude mono-crystal growth to proceed. Instead, unsteady thermodynamic conditions will initiate single crystal growth from the heterogeneous region of CaF_2 – CaO phase diagram. As a result, it appears a great number of fine fluorite crystals with higher temperature of crystallization than T_{crys} at the CF, which produce an intensive light-scattering and the grown crystals turn out white-milk in colour, being fully opaque within UV–VIS range.

To stabilize the growing equilibrium in accordance with criterion (18), one can lower appropriately V_{cryst}, that is, the SC. However its excessive decrease turns out unacceptable for industrial crystal production and, besides, may cause considerable evaporation and/or decomposition of the molten material with following break in stoichiometry owing to loss of F^- from anionic sub-lattice. Thus for eliminating the CMSc due to the presence of CaO, mostly oxygen contaminants, involved in Ca oxidation, have to be removed before T to exceed 880 ºC whereat temperatures the rate of chemical oxidation to increase dramatically. Alternatively, the solubility of mostly oxygen-containing contaminants in the solid phase may be risen up considerably by introducing definite amount of tri-valence RE ions into the lattice since their extra-charge leads to local compensation of the negative charge of O^{2-} and they turn out incorporated into anion sub-lattice. Combining the two methods discussed, one may anticipate the established constitutional T-gradient to remain satisfactory low so that it may be efficiently compensated by ensuring opposite steep axial T-gradient along the FU and by setting moderately low SC.

According to criterion (18), the presence of RE or any other metal impurities, the effective segregation coefficient of which remains closed to unity, should not contribute for enhancing the CMSc effect in case their concentration does not exceed several hundreds of ppm in starting fluorspar whereat they could not be treated as second solid solution component. However, in many cases when UV-grade CaF_2 has been grown, the RE impurities turns out rather undesired being embedded into the lattice since they act as optical active centres of specific light absorption. At this junction, not embedment into the lattice, but efficient removal of these impurities from the CZ appears obligatory for growing crystals with needed optical characteristics.

It should be taken into consideration that melt supercooling, not related to the purity in CZ, can arise being caused by appearance and constant rise up of radiation flow throughout the growing transparent crystal, surpassing increasingly the conductive flow towards the cold furnace zone.

7.2 Interface stability during the growth of $Ca_{1-x}Sr_xF_2$ crystals

7.2.1 Growing runs

Two growing runs are performed by using correspondingly the two types of multicamera crucibles placed in BSGS thermal field determined by two limiting cases as regards the mutual disposition of the movable part (batch of rings fixed on crucible stem) and fixed part (a thin liner, 15 cm long, mounted through the bore of SD, 2.47 cm thick) of the MoShS. Thus, 9 rings participate in run*1* whereas no rings are slept on the stem in run*2*. Besides the SC is chosen different for the two runs altering in step-wise manner (between 2 and 3 mm per hour – for run*1*) or being constant (equal to 6 mm per hour – for run*2*) – **Fig. 1**. Such SC regimes are thought being in conjunction with the two limiting cases for MoShS effect. These cases concern

total re-distribution for heat flux throughout the load. It is supposed the liner to play a role of a long pseudo-diaphragm that restricts the radial heat losses, reflecting the emission from both, the lateral surface of moving crucible and the lower furnace heater. On the other hand the fixed rings below the bottom of moving crucible cause – at a given instant – a jump in the current gradual alteration of the vertical (axial) to radial heat exchange, depending on crucible position into the FU. Initially, when crucible with the number of rings on its stem is being fixed on the starting position into Z1, all rings turn out within the liner region (LR). At this junction, after stabilization of power supply, some amount of heat will be accumulated in between crucible bottom and the upper batch's ring that causes an increase in temperature into the load, thus providing more frugal melting of the charged portions. Further, by withdrawing the crucible towards Z2, the rings will pass consecutively outside the LR, whereat the lateral heat transport from the load increases. That way, the total heat flux throughout the load turns out facilitated, leading to T-drop down therein whereat the CF will shift downwards correspondingly. At the absence of rings below crucible bottom such re-distribution of the total heat flux should not occur and only the liner will affect the CF position.
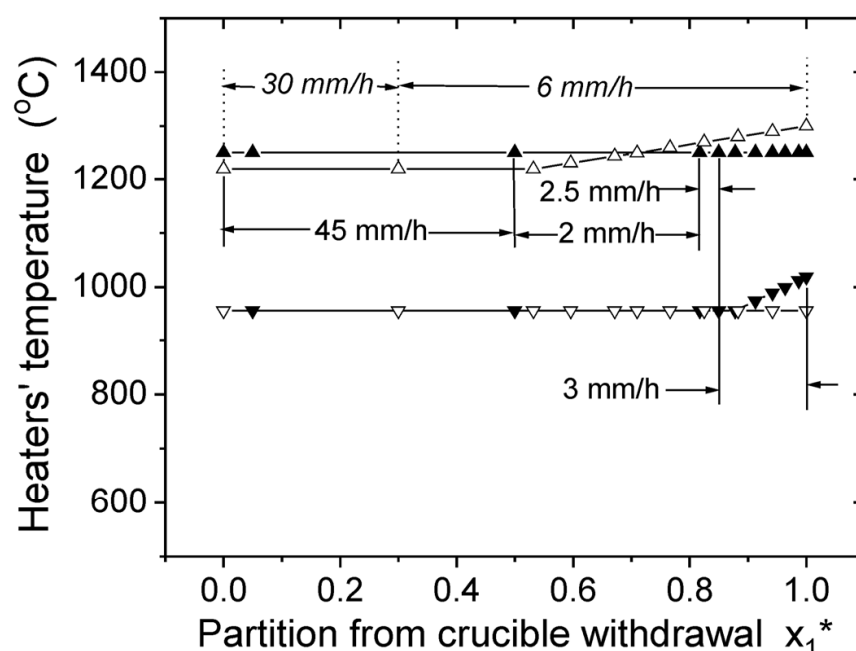
Fig. 1. Temperature regimes for BSGS-furnace zones during the growth of calcium–strontium fluoride mixed crystals: run 1 (2–2.5–3 mm/h): (▲) – T_1(Z1), (▼) – T_2(Z2); run 2 (6 mm/h): (△) – T_1(Z1), (▽) – T_2(Z2). The intervals for set crucible speed are marked as well.

The initial proportions of CaF_2 to SrF_2 are controlled so that x in the grown $Ca_{1-x}Sr_xF_2$ solid solutions to vary within 0.007 and 0.307 (run1) and 0.383 and 0.675 (run2).

7.2.2 Phase diagram

The $Ca_{1-x}Sr_xF_2$ phase diagram when the used fluorspar (concentrated to 99.6 wt.%) contained some insoluble amounts of silicon, aluminium and iron oxides and traces of other metal impurities where the RE varied up to 100 ppm, is shown on Fig. 2. It is seen both liquidus and solidus curves pass through aezotropic minimum at $x \approx 0.35$ sifted to lower Sr concentrations and considerably low temperature ($T_{Lid} \approx 1620.9$ K) as comparing az.p. $x \approx$

0.42 ($T_{Lid} \approx 1645$ K) – established by Klimm and co-workers (2007) utilizing pure chemical compounds for the end members (see Fig. 3 in Mouchovski et al. (2011)).
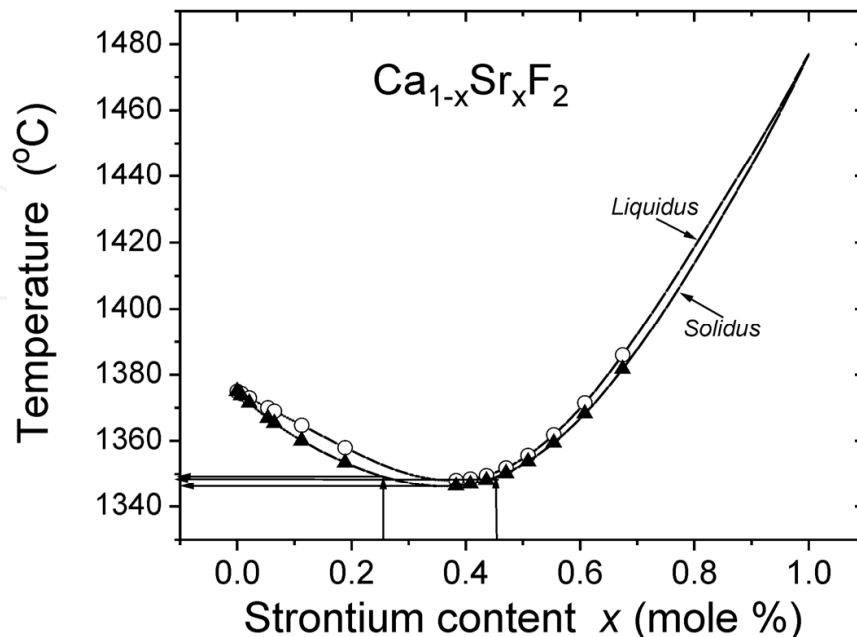

Fig. 2. Binary system of CaF_2 – SrF_2 where for CaF_2 end member is used fluorspar, mined from Slavyanka Bulgarian fluorite deposit, with m.p. (1375 ± 10) ºC; SrF_2 is "suprapur" quality (supplied by Merck), with m.p. 1477 ºC. For carried out growing runs by arrows are shown: ΔT_{sol} variation of 2.8 K around the aezotropic point of 1619.9 K for Δx within 0.25–0.45, (x = 0.352 at az.p. minimum). The corresponding ΔT_{liq} variation of 5.7 K lies within 1625.6 and 1619.9 K.

At this junction relevant alterations in calculated compositional dependences for critical stability function $F(x)_{crit}$, interdiffusion coefficient $D_{Ca/Sr}$ and equilibrium segregation coefficient k_o will occur. They are grounded on theoretical expression (13) that relates $D_{Ca/Sr}$, $F(x)_{crit}$, and V_{cryst}/G-ratio wherein – as discussed below – the real T-gradient ahead the CF may change considerably with crucible withdrawal into a thermal field with altering axial T-gradient. At the same time the real CR differs from the set SC depending on the shift in CF-position x. Moreover, as shown experimentally elsewhere (Mouchovski et al., 2011) the crystallization in each camera with different composition for loaded mixture (different x) will start at different crucible position $x_1{}^*$.

As regards k_o, according to formula (7), it depends in complex way indirectly on x via $L_{melt}(x)$ and $T_{melt}(x)$ functions.

7.2.3 Equilibrium coefficient of segregation

This is important parameter since indicates how the differences between molar concentrations of liquid and solid phases for the second (Sr) component at the $IF_{L/S}$ alter in accordance with mixtures' composition, x. As seen (Fig. 3) the calculated curve cross the basic line $k_o = 1$ at $x \approx$ 0.35 indicating that compositions not far from this value appear especially appropriate for growing to proceed at minimum CMSc effect. Nearly constant slope of the curve is observed within $0.13 \leq x \leq 0.58$ whereas at higher Sr content k_o stays in practical uniform, varying

slightly around 1.2, thus revealing some rejection of the second components ions by moving CF. At infinitively low Sr-concentrations k_o declines steeply to limiting value of ≈ 0.79.
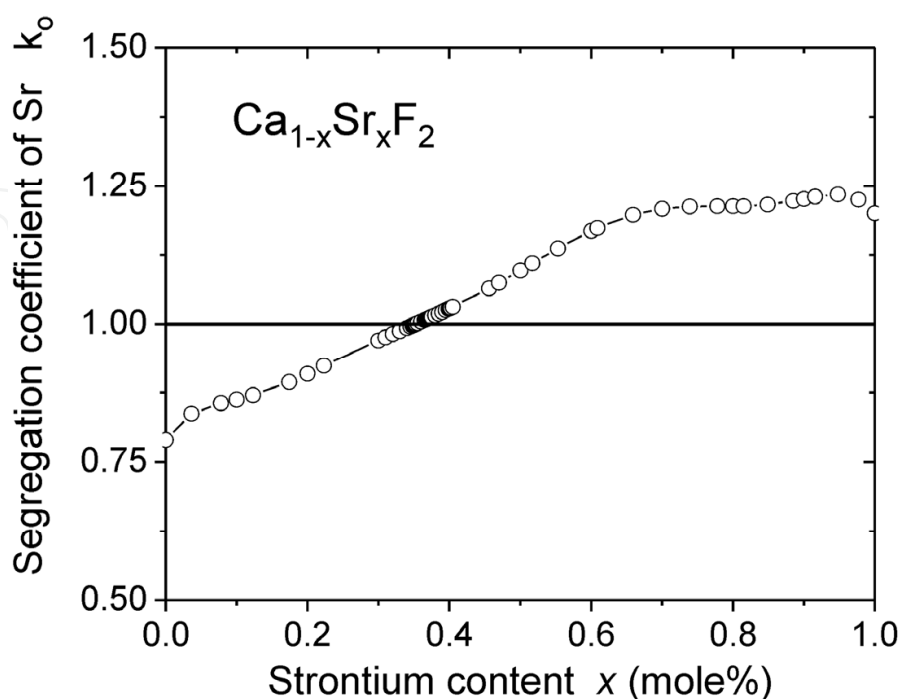

Fig. 3. Equilibrium segregation coefficient of Sr as a function of its content in simultaneously grown batch of $Ca_{1-x}Sr_xF_2$ boules where fluorspar (m.p. of (1648 ± 5) K) is being used for CaF_2 end member.

7.2.4 Compositional dependence of stability function

As suggested by the view of the phase diagram on Fig. 2, the compositional dependence of stability function (Fig. 4), calculated on the base of run1+run2 dataset (17 points), reveals a clear minimum close to zero at $x \approx 0.47$ that means, the corresponding run2-boule should be grown at mostly favourable conditions as regards CMSc effect. For two other boules, where x is positioned not far from the minimum (0.383 and 0.55, respectively), $F(x)$ remains below 1.6 K that can be considered being acceptable reduction of the CMSc effect. Only boules with extremely low x or $1-x$ should be at similar favourable growing conditions.

Surprisingly, the established $F(x)$ minimum at $x \approx 0.47$ differs from az.p. at $x \approx 0.35$. The reason for such divergence lies in the fact that the critical values for stability function depends as well on the partition from crucible withdrawal x_1* via the dependence on this variable for the ratio of axial T-gradient to CR, multiplied by $D_{Ca/Sr}$. In turn $D_{Ca/Sr}$ depends on x_1* via the opposite ratio for these apparatus/runs factors, multiplied by $F_{crit}(x)$.

The complex functionality for both dependences requires their investigation as regards the two runs growing conditions.

7.2.5 Determination of the real axial T-gradient into the load

The magnitude of the real T-gradient ahead the CF, G_{CF}, depends on CF-shift upward or downward during crucible movement through the FU T-field, characterized by its axial T-

profile and relevant furnace gradient G_{fur}. Besides, the effective thermal conductivity for both solid and liquid phases and the interface transition resistance of the interface affect G_{CF}. At this junction a semi-empirical formulas, giving the alteration of these T-gradients are much better to be derived for each particular FU configuration instead to utilize speculatively any sophisticated thermal model developed for the purpose.
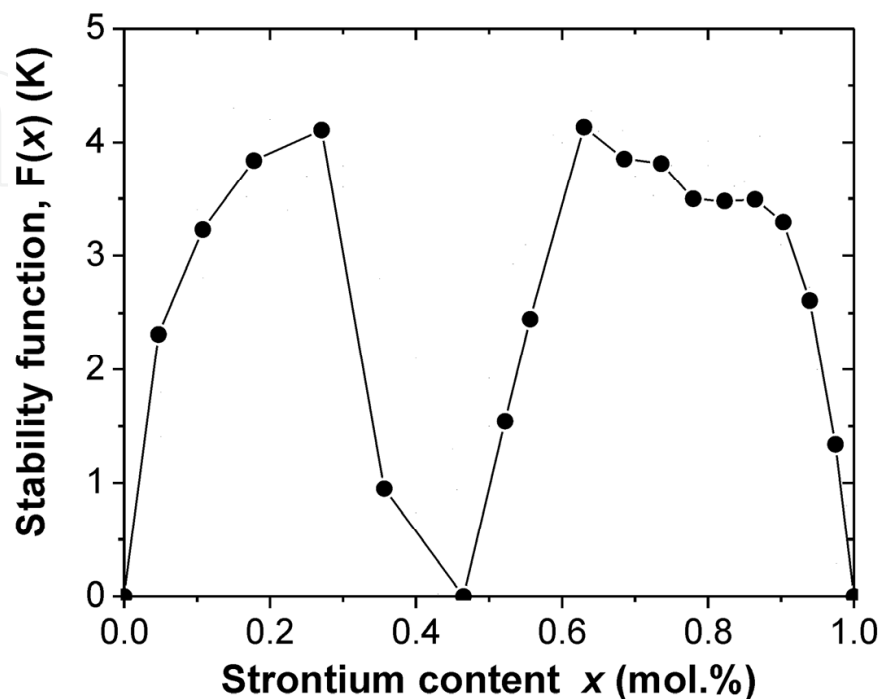

Fig. 4. Stability function $F(x)$ for $Ca_{1-x}Sr_xF_2$ system with CaF_2 m.p. 1648 K.

The first step here is determination of the axial T-furnace profile measured in empty crucible by moving downwards a high sensitive thermocouple and keeping a constant distance between its junction and the inner surface of crucible bottom. The power supply is being T-controlled by means of highly precise programmers/ controllers. The thermal field along the FU is established according to set MoShS configurations. The differentiated T-profiles (Fig. 5) reveal specific alteration for $G_{fur}(x_1{}^*)$ slopes along the FU. As seen for run1-conditions the slope of curve 1 rises up gradually. This is a result of the obtained parabolic shape for initially measured T-profile, which lowering branch is formed at the consecutive passage of the rings outside the LR. The role solely of the liner is apprehended as comparing curve 2 (no rings) to curve 1 (9 rings); the less steepness of curve 2 manifests the absence of rings results in facilitating the heat flux towards Z2. Nevertheless the slope seams being with sufficient steepness, attaining a constant value of 13.7 K/cm just below the AdZ, that to ensure stable, favourable conditions for normal growth to proceed.

Besides the slope, the absence of rings affects as well the position for T-profile that appears shifted more than 100 K to the lower temperatures as comparing the T-profile for curve 1. That means the crystallization should start at much higher position of the load – into Z1. To compensate such loss of heat into the load a relevant increase of power supply is being carried into effect (Fig. 6a, b) so that the growth to start and proceed more favourably in LR.

The correct assessment of CMSc effect requires G_{real} on G_{fur} dependence to be followed along the height of growing boules. First of all that means to be clarified the regularities those govern the CF position during the growth itself. As seen (Fig. 6a, b) the CF-position depends substantially on the composition of solid solution crystals. Thus for covered interval, $0.007 \leq x(Sr) \leq 0.307$, run1 conditions determine the CF-positions being either entirely in Z1 ($x = 0.007$), that means convex CF shape, or to vary around the lower (boundary) cross section of the AdZ ($x = 0.307$) whereat the relevant shape will tend to become slightly concave.

Run2 conditions ensured much larger alteration in CF-positions – from entirely above Z2 ($x = 0.675$) to mostly in Z2 ($x = 0.383$). The best appropriate composition seems to be for the crystal with $x = 0.55$ (Fig. 6b) where the CF changes gradually and insignificantly, being entirely within the AdZ that presupposes its shape to be kept nearby planer.

On each one CF-position into the FU corresponds particular slope of both, the set furnace T-gradient G_{fur} and relevantly established real T-gradient ahead the CF, G_{real}. Thus it can be followed the alteration in G_{fur}, respectively G_{real}, during the growth of a boule with definite height, h_{boule}, presented in dimensionless form: $h_{boule}* = h_{boule}/l_{crmov}$.

For the accomplished two runs: $z_{incon} = 11$ cm while $l_{crmov} = 17.7$ cm (run1) and 20.6 mm (run2).
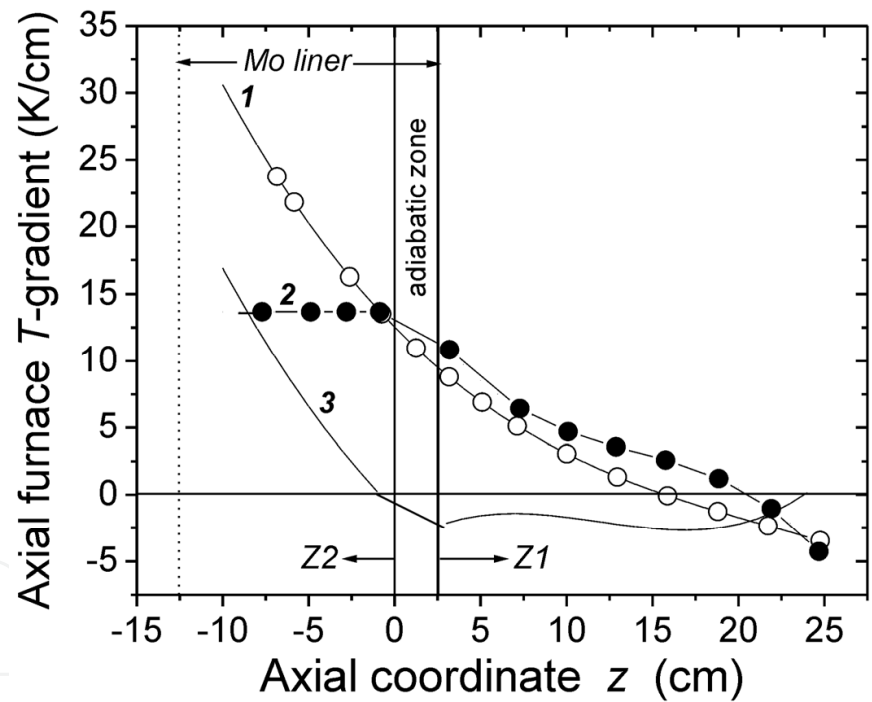
Fig. 5. Axial T-gradient in empty crucible measured along BSGS FU at two sets of thermal conditions. The data points are fitted by high order polynomials: curve 1 – (○) liner + 9 rings on crucible stem; curve 2 (●) – liner without rings Curve 3 – the difference between curve 1 and curve 2.

At boundary values for Sr-content x in the grown solid solution system – boules 0.007 and 0.307 (run1) and 0,383 and 0.675 (run2) – the maximum, mean, and minimum G_{fur} (G_{real}) are given in Table 1 while the T-gradient alterations are shown in Fig. 7. The initial analysis is grounded on the average values for G_{real} (column 7 in Table 1) as the maximal deviation is being estimated using the one and the same reduction factor of 2.8 for reduction of G_{fur}

within the LR that cover AdZ and the upper section of Z2. Thus reduced gradient is considered to stay constant within a particular section of the LR. The average G_{fur}-values are given together with their maximum deviation.
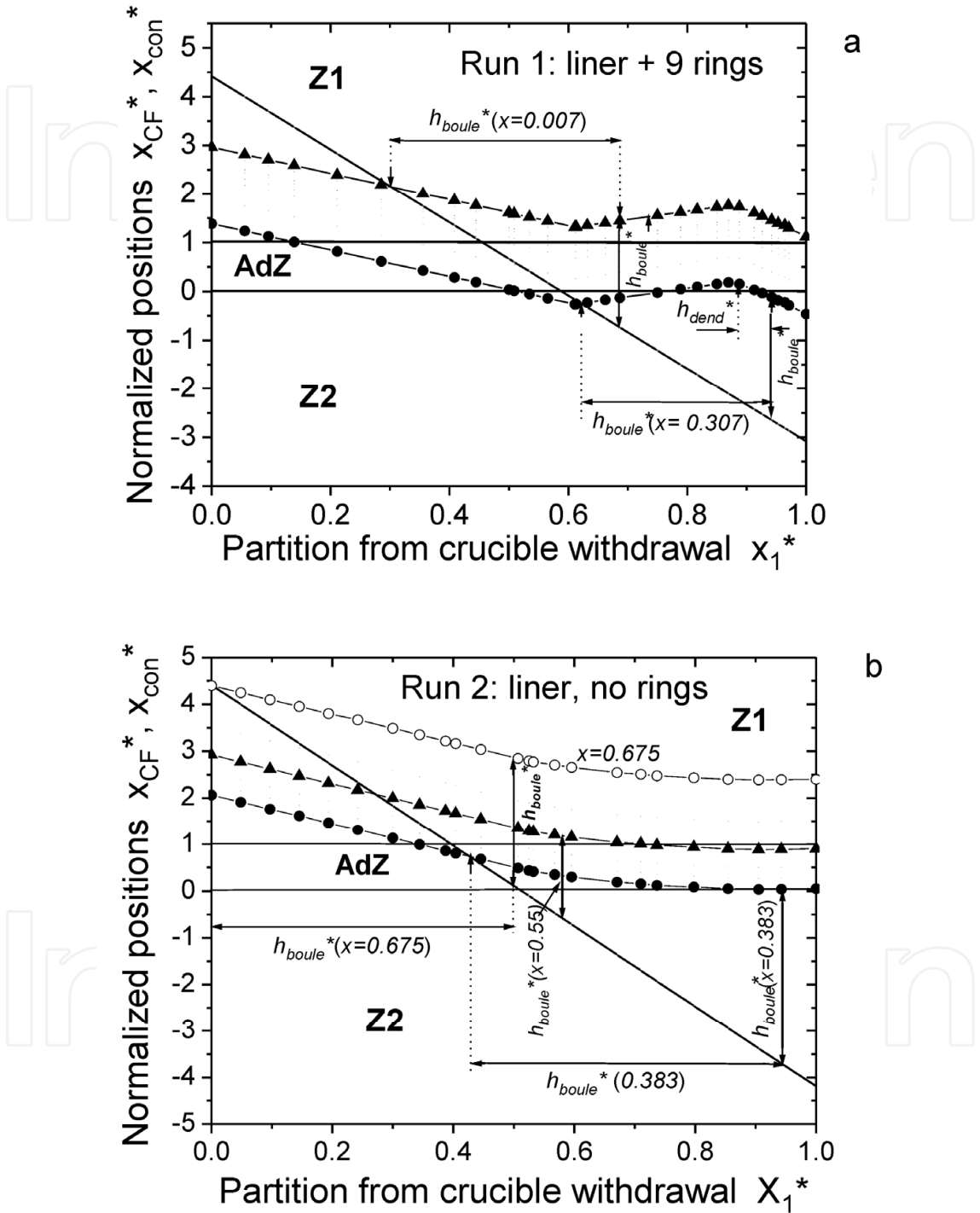

Fig. 6. a, b. Normalized positions of the CF and cameras tips' cross-section $x_{con}*$ along the FU depending on the partition from crucible withdrawal during two growing runs of $Ca_{1-x} Sr_x F_2$ boules where Sr content x varied between: **a** (run 1) – 0.007 (▲) and 0.307 (●). **b** (run 2) – 0.383 (●), 0.55 (▲) and 0.675 (●). The lines describing $x_{con}*$ are given appropriately. The total boules' height is shown, normalized by AdZ thickness, $h_{boule}* = h_{boule}/l_{Adz}$.

Comparing the alterations in G_{real} for the two runs (Table 1 and Fig. 7) one can see divergence from G_{real}(Av) for run2-boules that attains 53% but only for those boules wherein the Sr appears clearly the dominant component, since then the boules should be grown at permanently increasing T-gradient. At lowering the x around and below 0.5 the CF shifts in a manner the growth to proceed more and more at the flat T-gradient section so that the divergence from the average falls down rapidly attaining the insignificant 12% at x minimum of 0.383. For this run G_{real} should alter between 4.8 and 11.3 K/cm (x = 0.55). On the other hand the divergence for run1-boules varies between 27% (x = 0.307) and 42% (x = 0.007) but the first value is related to the lowest G_{real} average for this run of only 6 K/cm.

No. run	x(Sr)	x_1^* (from/to)	G_{fur}(min/max) (K/cm)	G_{fur}(av) (K/cm)	CF-position CF-shape	G_{real} (K/cm)
1	0.007	0.3	6.3	11±4.7	Z1 Convex	≈ 11±4.7
		0.68	14.0			
	0.307	0.62	12.5	17±4.5	Z2/AdZ/Z2 Cv/Plan/Cv	≈ 6±1.6
		0.94	21.4			
2	0.383	0.43	11.9	13.5±1.6	AdZ Planar	≈ 4.8±0.6
		0.94	13.7			
	0.554	0.27	8.3	11.3±3	Z1 Convex	≈ 11.3±3
		0.57	13.7			
	0.675	0	4.2	9±4.8	Z1 Convex	≈ 9±4.8
		0.5	13.1			

Table 1. Alteration in axial temperature gradient measured in empty crucible during the two runs of $Ca_{1-x}Sr_xF_2$ boules with different content. The assessed indirectly real T-gradient ahead the CF, G_{real}, is also given.
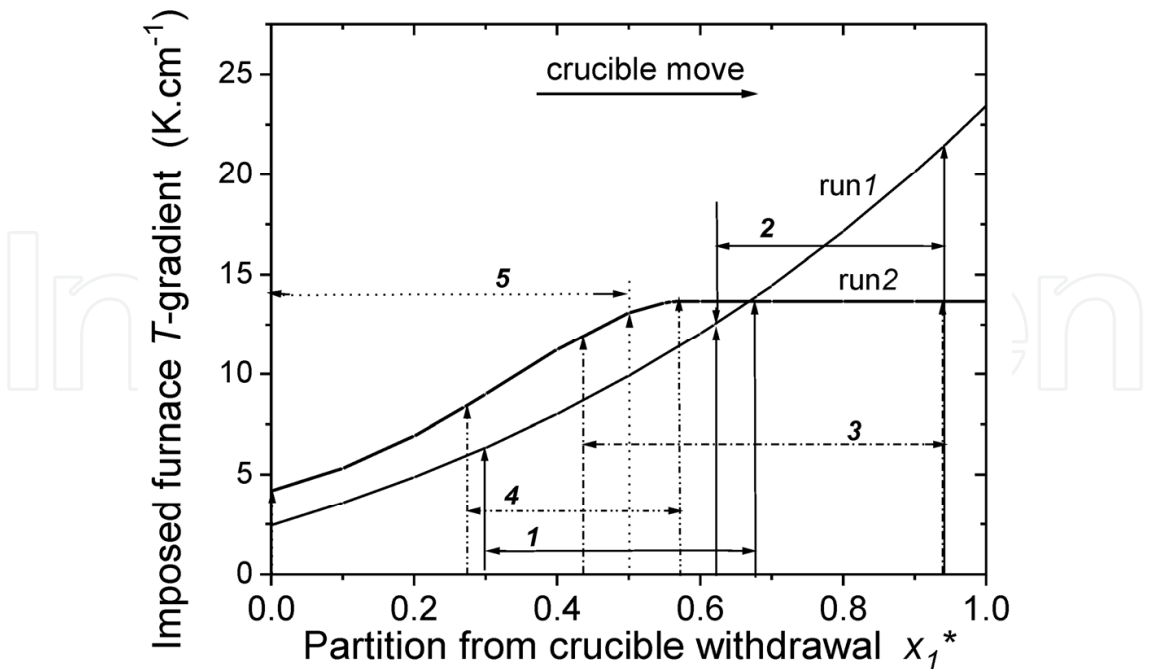
Fig. 7. Axial temperature gradient, measured in non-loaded multicameral crucible, as a function of crucible position during the two growing runs of $Ca_{1-x}Sr_xF_2$ boules with different content. Run1: 1 – x = 0.007 and 2 – x = 0.307; Run2: 3 – x = 0.383, 4 – x = 0.554 and 5 – x = 0.675.

Despite these common arguments assist the conducted analysis, its obligatory preciseness demands, however, both Sr to Ca interdiffusion coefficient and stability function dependences on the ratio of G_{real} to V_{real} being obtained by using corresponding fitting equations for $G_{real} = f_G(x_1^*)$ and $V_{real} = f_V(x_1^*)$. The first relationship follows directly from $G_{fur} = f_G'(x_1^*)$ shown in Fig. 7 by relevant reduction of 2.8 depending on whether the CF sifts inside or outside the LR (AdZ).

7.2.6 Determination of the real crystallization rate

The other factor, influencing the interdiffusion coefficient and, respectively the magnitude of stability function, is the real crystallization rate V_{real}. As discussed elsewhere (Mouhovski et al., 2011), this factor may differ – sometimes significantly – from the set SC, V_{cru} in conjunction with the altering thermal conditions into the load where the shift in CF-positions at constant furnace supply should determine corresponding divergences of V_{real} from V_{cru}. Nevertheless, as illustrates Fig. 6, V_{real}^*, vs. x_1^* dependence should stand one and the same for all boules since they have been grown in practical at equal conditions where one the same relative CF-shift occurs in all cameras at any crucible cross-section. As seen for both runs in study (Fig. 8) the real CR remains less than that of the SC up to the moment when the cameras' tips cross-section passes into Z2.

Specifically for run1 the surge of V_{real}^* up to 25% above 1 can be explained with abrupt enlargement for the total heat flux towards Z2 caused by a sharp decrease of the relevant effective thermal resistance, which constitutional radial part just disappears when all the 9 rings move at positions in Z2 below the lower boundary cross section of LR.

In case no rings is being fixed on crucible stem (run 2), an extra-heat release in radial direction starts significantly earlier, when the crucible bottom plane approaches the lower boundary section of the AdZ. Then the further crucible withdrawal is peculiar in approaching approximately constant acceleration of the V_{real}^* (Fig. 8) Such behavior is a consequence of the rise of 5 K/h imposed on the upper heater temperature T_1 (Fig. 1) whereby additional heat is supplied and flows into the inside of the upper load section. This way the heat losses resulting from the move into Z2 by a gradually enlarging lateral surface of the crucible are compensated with a surplus that causes a relevant downward shift of the CF corresponding to the observed constant increase of V_{real}^*. The smooth transition of a constant rate below the SC to a rate slightly in excess of SC is a ground for normal growth of boules having high optical quality.

The studied dependence manifests completely different behavior in case a gradual rise of 8.6 K/h is being imposed to lower heater temperature T_2 (Fig. 1, run1) for compensating the heat losses occurring through the movement into Z2. This manner it turns out not possible to adjust V_{real}^* to the favorable region around unity; the chosen heat increase is rather high leading to such fast lowering for CF-position that push V_{real}^* to decline abruptly to values far below 1 and even for a while it stays below 0 (Fig. 8, run1). As a result of this procedure the $IF_{L/S}$-stability as well as the normal growth would both be severely disturbed due to the development of a strongly concave shape to the CF causing increased impurity incorporation and more pronounced supercooling effect. Besides a small portion nearby the surface of the already grown boules melts again when V_{real}^* drops below zero, a phenomenon which would create additional growth anomalies and failure in crystal

structure. Hence one may anticipate the top section of some run*1*-boules to possess significantly worse values for the main optical characteristics as compared to those ones of the lower boules' sections.
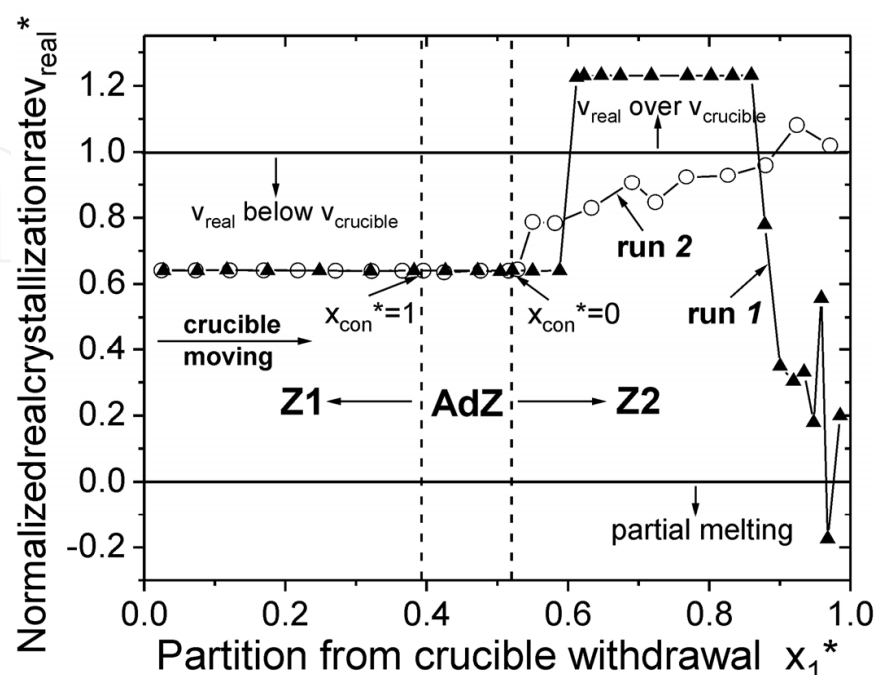

Fig. 8. Relative alteration of the real crystallization rate during two growing runs carried out under different thermal conditions for a series of $Ca_{1-x}Sr_xF_2$ boules.

7.2.7 Determination of interdiffusion coefficient

Calcium to strontium interdiffusion coefficient $D_{Ca/Sr}$ – according to formula (11) – depends primary on the critical value of stability function $F(x)_{crit} = m.\Delta x$ that has to be determined from the compositional phase diagram for studied solid solution system (Fig. 2). Besides, being proportional to this purely substantial thermodynamic factor, $D_{Ca/Sr}$ is a linear function of the ratio V_{real}/G_{real} of the real CR to real T-gradient established ahead the moving CF. Despite this ration seems being depended solely on the imposed growing conditions by the set SC and longitudinal T-gradient in the furnace, both – the real CR and the real T-gradient – appear functions of CF-position in each particular camera, which in turn, depends on the composition of the loaded portions/grown boules. At this junction the chosen variations in apparatus factors for the two runs cause considerable differences between corresponding values for $D_{Ca/Sr}$ (Fig. 9). Hence, in the cases under consideration to take an average value for this important mass-transport parameter in stability function formula and relevant CMSc criteria may lead to incorrect assessment about the growth mechanism expected.

Indeed, the presented in Fig. 9 five representative curves for the two runs differs substantially each other. Such result means the product of critical stability function $F(x)_{crit}$ and V_{real}/G_{real}-ratio affects in complex way and mostly considerably the interdiffusion for the two types alkali earth cations into building in fluorite lattice. Specifically two order of magnitude differences are found out at $x = 0.6$ for run*1*/run*2* ratio. Nevertheless the run*1* dataset within $0.62 < x < 0.94$ interval show a trend for fast lowering $D_{Ca/Sr}$ owing to a

combined effect of decreasing $F(x)_{crit}$ and increasing G_{real} while the alteration of V_{real} stays with less importance. Again relatively large values for $D_{Ca/Sr}$ ($\approx 4 \times 10^{-4}$ cm^2 s^{-1}) are found for run2 at x within 0.62–0.86 that is due, evidently, to established low but constant real T-gradient. Here the abrupt lowering of V_{real} starts to influence on $D_{Ca/Sr}$ only at $x > 0.86$. It seems the slowest, nearly constant interdiffusion to occur under run2-conditions in the boule with a largest Sr-content ($x = 0.675$) since then the G_{real} is equal approximately to set furnace T-gradient, G_{fur}, while the V_{real} to $V_{crucible}$ ratio is being maintained uniformly below 1 (0.64) during the whole run.
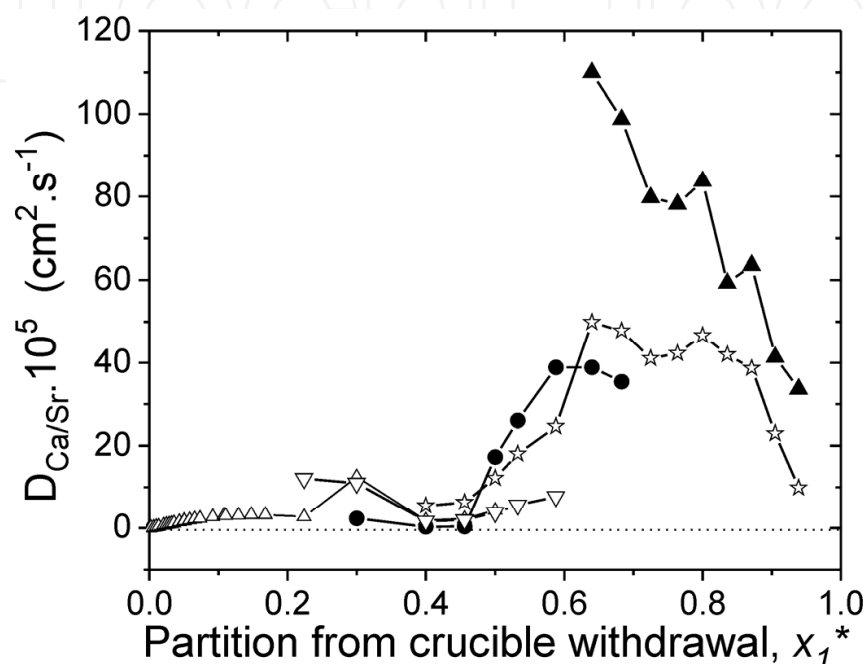
Fig. 9. Interdiffusion coefficient in growing of Ca$_{1-x}$Sr$_x$F$_2$ solid solution system as a function of the partition from total crucible withdrawal, x_1^* at different strontium content x in the simultaneously grown boules under particularly chosen thermal conditions (see Fig. 1). Run 1: ($\bullet$) – $x = 0.007$; ($\blacktriangle$) – $x = 0.307$. Run 2: ($\star$) – $x = 0.383$; ($\triangledown$) – 0.554; ($\triangle$) – 0.675.

The performed analysis of the compositional dependence for interdiffusion coefficient manifests how important is to be known (determined precisely or assessed correctly) all factors that influence this mass-transport coefficient so that the stability criterion to outline correctly the region of normal growth at minimum supercooling effect that may ensure simultaneous growing of boules – solid solutions of CaF$_2$–SrF$_2$ mixed system – with different composition.

7.3 Stability criterion and crystal quality

The unifying presentation of critical stability function vs. the partition from crucible withdrawal during the two growing runs (Fig. 10) appears especially convenient for comparative analysis. The calculated curve manifests certain similarity with the curve in Fig. 4 that, however, should not mislead the reader because the variables are completely different. Smoothing the curve, its extreme minimum of only ≈ 0.5 K appears within 0.4–0.46 that determines position of the crucible just before its middle cross-section. Around this minimum the boules should grow at very low melt supercooling but its exact position as

regards boules' height is compositionally dependent via really established local T-gradient and CR. All area below the curve outlines growing conditions with unacceptable level for melt supercooling.

Specifically at run1 conditions the F-function goes down steeply during the growth of approximately the first ⅓ of the height of the boules with utmost low Sr-content ($x \le 0.1$) as nucleation starts at relatively high $F(x_1^* = 0.3) = 3.7$ K ($x = 0.007$).

In accordance with curve's course the nucleation/growth conditions change dramatically for boules with higher x approaching the limiting value of 0.307 (run1) whereat the entire process will proceed at significant melt supercooling (3.5 K $\le F(x_1^*) \le 3.95$ K).
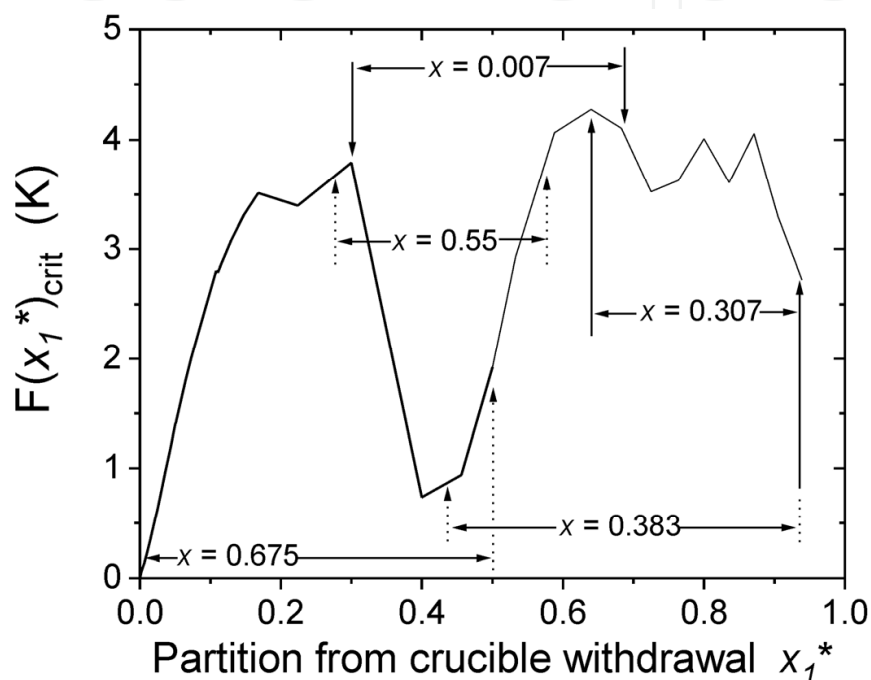
Fig. 10. Critical stability function $F(x_1^*)_{x=const}$ for calcium strontium fluoride solid solution system as a function of crucible movement towards Z2 for two specific run's growing conditions and parameter – strontium content into the grown boules. The limiting strontium concentrations for the two runs are marked by arrows: run1 – 0.007–0.307; run2 – 0.383–0.675. $x = 0.55$ corresponds to boule with the lowest light extinction measured within UV – NIR spectral range.

On the other hand the growth of both boules, referring to limiting Sr-content x of 0.383 and 0.675 (run2), should start at very low values for $F(x_1^*)$ but the function increases rapidly thereafter. Such behaviour suggests for fast deteriorating growing conditions. Hence the crystal quality for run2-boules can expect being worse as compared to that of run1-boules. Certain correlation is found analysing comparatively the light-extinction spectra obtained within the two series of windows between ser.1 (prepared from the lowest cylindrical boules' section and ser.2 (prepared from higher disposed section, distant at least to 0.6 cm from the first one. Nevertheless more precise analysis is being implemented using a new parameter, defined as the difference in stability function values determined at upper and lower boundary plane sections for given series windows, $\Delta F(x_1^*)$ that is being juxtaposed for particular boule to relevant discrete values of E_λ-spectra within UV, Vis and NIR (Fig. 11).
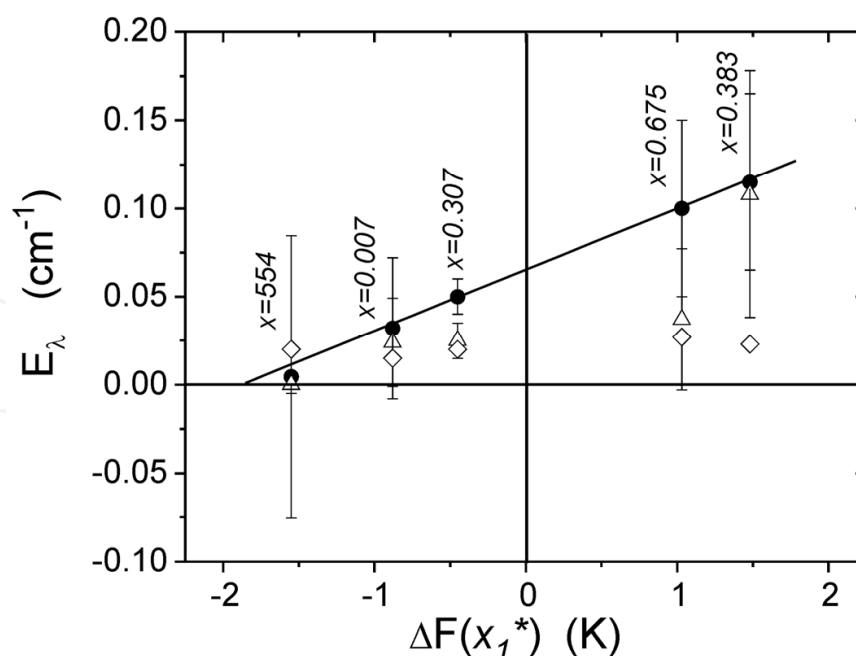
Fig. 11. Average light extinction for three λ within UV ($\bullet$), Vis ($\triangle$) and NIR ($\diamond$) spectral regions measured in ser.1-optical windows, finished from the lowest cylindrical section of the five representative boules vs. the difference in stability function values at coordinates corresponding respectively to upper and lower windows plane sections.

As seen, significant variations for E_λ are established along the thickness of only 0.6 mm for ser.1-windows. Besides, the found deviations differ in conjunction with spectral region considered. Interestingly a linier dependence is fitted for dataset obtained into UV region that predetermines certain local structural inhomogeneities along the whole height of the grown boules. To check this suggestion all 17 grown boules are testified as regards possible longitudinal alteration of their optical transmission measured in corresponding pairs of windows. Relevantly calculated differences between coefficients of light extinction, ($E_{\lambda(win2)}$ – $E_{\lambda(win1)}$), are followed as a function of corresponding average quantities $E_{\lambda(win1+win2)/2)}$ for each particular boule.

The data points obtained (Fig. 12) are found to scatter significantly within interval of less than 0.1 cm-1 as mostly differences ($\approx$ 65%) appear with positive sign that stands for gradually degenerating optical quality towards the tip of corresponding boules. It is seen as well the deviations of positive values from zero line to scatter more broadly as comparing those for the boules where the sign of ($E_{\lambda(win2)}$ – $E_{\lambda(win1)}$) stays negative.

The linear fit reveals a very strong correlation in the VIS and IR with R > 0.94 that becomes significantly weaker in the UV (R $\approx$ 0.65) [100]. The later indicates a higher sensitivity to crystal imperfection from any variations in growth conditions, manifested by relevant alteration of the stability function, at the shorter wavelengths where even the smallest structural defects influence on the regularity of the crystal lattice. This result is in accordance with the followings in Fig. 10 where the light extinction just in the UV region depends essentially linearly on the newly introduced variable $\Delta F(x_1^*)$, that gives the direction of the relative $F(x_1^*)$ alterations. Hence the development of supercooling effect – by its amplifying or attenuating – gains a decisive importance upon the regularity of crystal lattice formation.
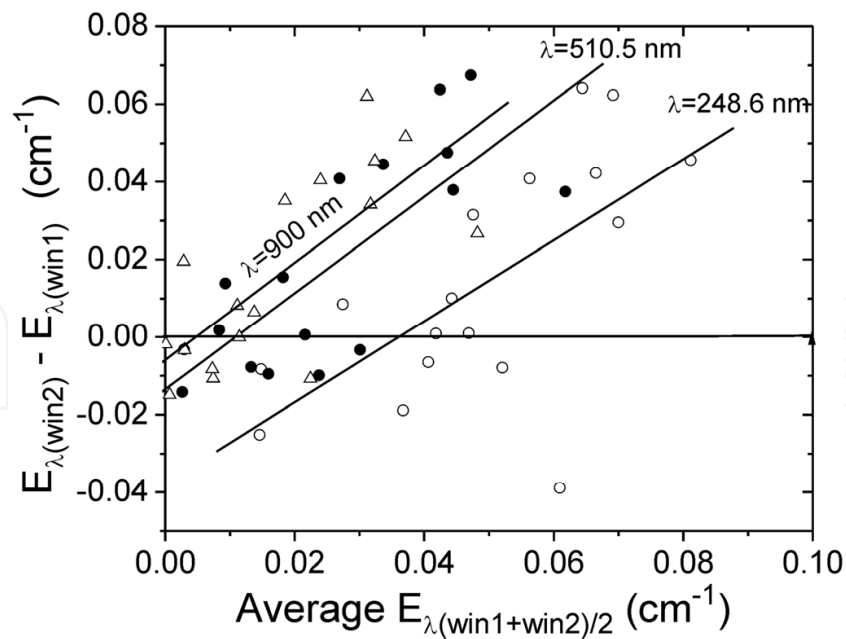
Fig. 12. Difference in light extinction coefficient obtained for particular wavelength within UV–IR in pairs of windows prepared from non-adjacent parallel sections of the grown boules with different content x vs. average light extinction for corresponding pairs of windows at λ: 248.6 nm ($\circ$), 510.6 nm ($\bullet$), and 900 nm/6.45 µm ($\triangle$).

7.4 Normal growth criterion

The criterion for normal growth is being applied in order to assess how effectively the latent heat of fusion L_{molt} can modify the growth mechanism for studied solid solution fluoride
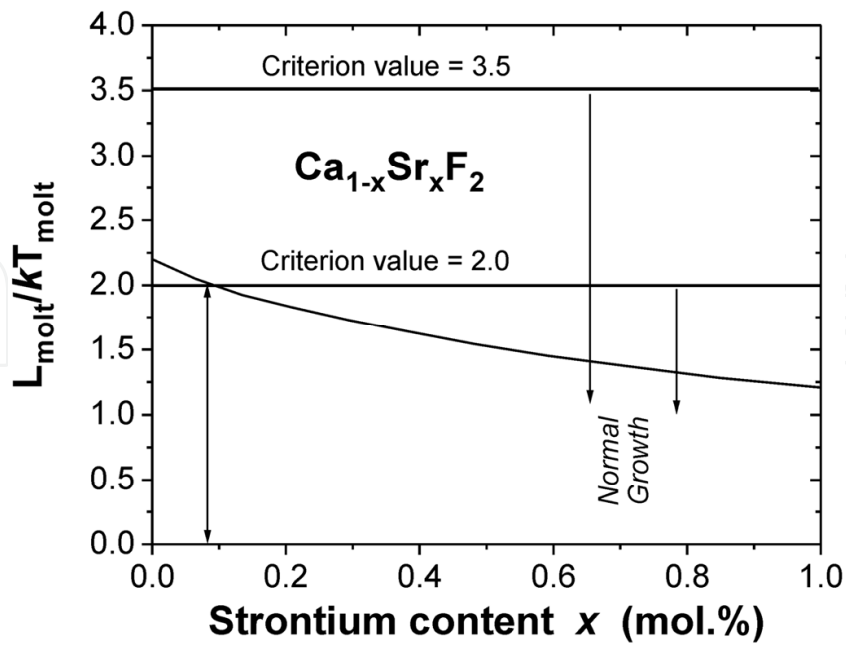
Fig. 13. Compositional dependence of normalised latent heat of fusion for studied $Ca_{1-x}Sr_xF_2$ solid solution system. Two cited in the literature boundary values for proceeding of normal growth are denoted correspondingly.

system, which involves single normal isotropic growth to a strongly anisotropic one with a resulting laminar distribution of the second (Sr) component. It is seen (Fig. 13) the studied L_{molt}/kT compositional dependence crosses the criterion lower limiting value of 2.0 at $x \approx 0.08$ mole% whereas the curve is positioned entirely below the criterion upper limiting value of 3.5. At this junction one may suppose only two of run*1*-boules, the composition of which satisfies $x \le 0.08$ mole% condition, being grown, eventually, under cellular, strongly anisotropic growth mechanism. However the results from the optical measurements and several microscopic observations (Mouchovski et al., 2011) do not suggest such mechanism to initiate dendroidal/cellular sub-structure in any of investigated sections (optical windows) for studied boules. Hence, taking criterion upper limit of 3.5, it may be concluded the growing conditions for both runs were ensured proceeding of normal growth in the used multicameral crucibles.

8. Conclusion

Simple constitutional melt supercooling criterion for liquid to solid interface stability may be applied for reliable assessment of the most favourable growing conditions established in batch growth, by optimised BS technique, of $Ca_{1-x}Sr_xF_2$ boules with broadly varying composition. The stability function representing the supercooling effect reveals specific compositional dependence, following the alterations arisen in CaF_2–SrF_2 phase diagram when for CaF_2 is being used fluorspar with different m.p. than that of the chemical reactive. The critical values for stability function vary along the boules in accordance with their composition, determining different positions wherefrom the crystallization starts to propagate. These interfering phenomena are grounded on specificity of the thermal field, established into loaded crucible, which can be controlled effectively by original appliance in growing apparatus for regulating the heat exchange into the furnace unit.

It is possible the axial T-gradient, measured into the furnace, being reduced in accordance with the positioning of the crucible into the thermal field established, to be recognized as the real T-gradient in stability function presentation.

The differences in stability function increasing or lowering values along definite sections of the boules, being linearly dependent on the relevant changes – positive or negative, respectively – in the key optical characteristics, bring significant valuable information about expected quality of mixed fluoride crystals with different composition, grown simultaneously at varying growing conditions. At that, the real crystallization rate can differ significantly on the set speed of crucible, thus imposing a need for supplementary correction in stability function magnitude along the boules' height.

Both, the alteration in stability function together with changeable ratio of real crystallization rate to real T-gradient, lead to great differences for interdiffusion behaviour in each section of the grown boules. This result should draw the researchers attention not to take automatically the view for constant interdiffusion processes during the growth of such complex solid solution fluoride systems but to provide supplementary investigation especially in cases of simultaneous growth of boules with different compositions.

The exact position of equilibrium segregation coefficient and interdiffusion coefficient into compositional space is of substantial importance for correct determination of stability

function magnitude and application of corresponding supercooling criterion. The deviation of equilibrium segregation coefficient from unity may attain 20% at compositions with small or large *x* that suggests considerable re-distribution in cation sub-lattice, predetermining stoichiometric changes along the boules' height.

The simple supercooling criterion manifests as well the importance for removing of any oxygen-containing contaminants from the crystallization zone (CZ). In case fluorspar is being used as starting material for growing of single or mixed fluoride compounds, it may be processed on original high-*T* procedure, involving some scavenger's reactions in high vacuum, for substantial reduction – up to trace concentrations – of mostly residual metal oxides, product of decomposition of the accessory minerals, as well as deeply adsorbed on fluorspar grains oxygen anions. Possible penetration of ionised oxygen and water vapour molecules from vacuum ambient to melt bulk can be suppressed considerably when crucible construction provides Knudsen diffusion to dominate into the channels, relating the free spaces inside the crucible.

According to the simple supercooling criterion all impurities with effective segregation coefficient remaining sufficiently close to 1 (as appears all RE elements) and level of concentration within ppm-range do not cause any supercooling effect of significance.

The followings from applying the simple supercooling criterion should be apprehended cautiously since the high transparency for growing solid solution fluoride crystals and the semi-transparency of their melts within relatively large spectral range may change radically the thermal fluxes throughout the load leading to supplementary supercooling ahead the CF, the effect of which should be subject to analysis.

9. Acknowledgements

10. References

Alfintzev, G.A. & Ovsienko, D.E. (1980). Peculiarities of melt growing crystals of substances with various entropy of fusion. *Rost Kristallov* (Nauka, Moskwa), Vol.13, 121–123 (in Russian), ISBN/ISSN: 0485-4802.

Chalmers B. (1968). *Principles of solidification*, John Wiley & Sons, New York.

Chern'evskaya, E.G. & Anan'eva, G.V. (1966). Structure of CaF_2-, SrF_2-, and BaF_2-Based Mixed Crystals, *Fizika Tverdogo Tela* (Leningrad), Vol.8, No.1, 216–219 (in Russian), ISSN 1063-7834.

Chernov, A.A. (1984). *Modern Crystallography III. Crystal Growth* (Springer Ser. Solid-State Sci.), Vol.36, Springer, Berlin, Heidelberg 1984).

Deshko, V.I.; Kalenichinko, S.G.; Karvatzkii, A.Y. & Sokolov, V.A. (1990). Stability of temperature conditions during vertical directed crystallization of calcium fluoride

at radiative-conductive heat exchange. *Optico-mehanicheskaya promyshlennost*, No.1, 46–48 (in Russian), ISSN: 0030-4042.

Deshko, V.I.; Karvatzkii, A.Y.; Sokolov, V.A. & Hlebnikov, O.E. (1986). Temperature distribution in crystallization furnace at continuous growth of calcium fluoride crystals. *Optico-mehanicheskaya promyshlennost*, No.8, 28–31 (in Russian), ISSN: 0030-4042.

Djurinskij, B.F. & Bandurkin, T.A. (1979). Regularity in properties of lanthanides into inorganic materials, *Izvestiya Akademii Nauk SSSR, Neorganicheskie materialy*, Vol.15, 1024–1027 (in Russian), ISSN: 0002-337X.

Fedorov, P.P. (1991). Association of Point Defects in Non Stoichiometric $M_{1-x}\ R_xF_{2+x}$ Fluorite-Type Solid Solutions, *Bulletin of Society Catalan Cien*, Vol. 12, No. 2, 349–381.

Fedorov, P.P. (2000). Heterovalent isomorphism and solid solutions with a variable number of ions in the unit cell. *Russian Journal of Inorganic Chemistry*, Vol. 45, No. 3, 268–291, ISSN PRINT: 0036-0236. ISSN ONLINE: 1531-8613.

Fedorov, P.P.; Buchinskaya, I.I.; Ivanovskaya, N.A. et al. (2005). CaF_2-BaF_2 Phase Diagram, *Doklady Akademii Nauk*, Vol. 401, No.5, 652–654 (in Russian), ISSN PRINT: 0869-5652.

Fedorov, P.I. & Fedorov, P.P. (1982). *Grounds of technology for production of super-pure substances*, MIHM, Moskwa (in Russian).

Fedorov, P.P.; Turkina, M.; Meleshina, V.A. & Sobolev, B.P. (1988). Conditions of formation of cellular sub-structure in mono-crystals solid solutions inorganic fluorides with fluorite structure. *Rost Kristallov*, (Nauka, Moskwa), Vol.17, 198–216 (in Russian), ISBN/ISSN: 0485-4802.

Ito, M.; Goutaudier, Ch.; Guyot, Y.; Lebbou, K.; Fukuda, T. & Boulon, G. (2004). Crystal Growth, Yb^{3+} Spectroscopy, Concentration Quenching Analysis and Potentiality of Laser Emission in $Ca_{1-x}Yb_xF_{2+x}$, *Journal of Physics: Condensed Matter*, Vol.16, No. 8, 1501–1521, ISSN 0953-8984 (Print). ISSN 1361-648X (Online).

Jackson, A. (1958). Mechanism of growth, Liquid Metals and Solidification. *American Society for metals*, Cleveland, Ohio, 174–186, ISSN: 0096-7416.

Jackson, K.A. (2004). Constitutional Supercooling Surface Roughening. *Journal of Crystal Growth*, Vol.264, 519–529, ISSN: 0022-0248.

Kaminskii, A.A.; Rhee, H.; Eicher, H.J.; Bohaty, L.; Becher, P. & Takaichi, K. (2008). Wideband Raman Stoks and Anti-Stoks lasing comb in a BaF_2 single crystal under picosecond pumping. *Laser Physics Letters*, Vol. 5, No.4, 304–310, ISSN print: 1612-2011, ISSN electronic: 1612-202X.

Kazanskii, S.A.; Ryskin, A.I.; Nikiforov, A.E.; Zaharov, A.Yu.; Ougrumov, M.Yu. & Shakurov, G.S. (2005). EPR Spectra and Crystal Field of Hexamer Rare-Earth Clusters in Fluorites, *Physics Review B*, Vol.72, 014127-1–014127-11, ISSN: 0556-2805.

Klimm, D.; Rabe, M.; Bertram, R.; Uecker, R. & Parthier, L. (2008). Phase diagram analysis and crystal growth of solid solutions $Ca_{1-x}Sr_xF_2$, *Journal of Crystal Growth*, Vol. 310, No.1, 152–155, ISSN: 0022-0248.

Kuznetsov V.A. & Fedorov P.P. (2008). Morphological Stability of Solid-Liquid Interface during Melt Crystallization of $M_{1-x}R_xF_{2+x}$ Solid Solutions. *Inorganic Materials*, Vol. 44, No.13, 1434-1458, ISSN PRINT: 0020-1685; ISSN ONLINE: 1608-3172. DOI: 10.1134/S0020168508130037

Lucca, A., Debourg, G.; Jacquemet, M.; Druon, F.; Balembois, F.; Georges, P.; Camy, P.; Doualan, J.L. & Moncorge, R. (2004). High-Power Diode-Pumped $Yb^{3+}:CaF_2$ Femtosecond Laser, *Optics Letters*, Vol.29, No.23, 2767–2769, ISSN:0146-9592 (print) ISSN: 1539-4794 (online).

Maier, J. (1995). Ionic Conduction in Space Charge Regions, *Progress in Solid State Chemistry*, Vol.23, No.3, 171–263, ISSN: 0079-6786.

Mouchovski, J.T. (2006). *Growing of Optical Crystals of Calcium Fluoride*. Scientific Work, Central Scientific Technical Library at National Center for Information and Documentation, Sofia, Bulgaria (in Bulgarian), ISSN: 1312-6164.

Mouchovski, J.T. (2007a). Control of oxygen contamination during the growth of optical calcium fluoride and calcium strontium fluoride crystals, *Progress in Crystal Growth and Characterization of Materials*, Vol.53, 79–116, ISSN: 0960-8974.

Mouchovski, J.T. (2007b). Growing of mixed crystal compounds based on calcium and strontium fluorides, *Bulgarian Chemical Communications,* Vol.39, No.1, 3–8, 2007, ISSN: 0324-1130.

Mouchovski, J.T.; Genov, V.B.; Pirgov, L. & Penev V.Tz. (1999). Preparation of CaF_2 precursors for laser grade crystal growth. *Materials Research Innovations*, No.3, 138–145, ISSN (printed): 1432-8917. ISSN (electronic): 1433-075X.

Mouchovski, J.T.; Penev, V.Tz. & Kuneva, R.B. (1996). Control of the growth optimum in producing high-quality CaF_2 crystals by an improved Bridgman-Stockbarger technique. *Crystal Research and Technology*, Vol.31, No.6, 727–737 Print-ISSN 0232-1300. Online-ISSN 1521-4079.

Mouhovski, J.T.; Temelkov, K.A. & Vuchkov, N.K. (2011). The Growth of Mixed Alkaline-Earth Fluorides for Laser Host Applications. *Progress in Crystal Growth and Characterization of Materials*, Vol. 53, 1–41, ISSN: 0960-8974.

Mouhovski, J.T.; Temelkov, K.A.; Vuchkov, N.K. & Sabotinov, N.V. (2009a). Calcium strontium fluoride crystals with different composition for UV-laser application: control of growing rate and optical properties, *Compes Rendus*, Vol.62, No.6, 687–694, ISSN: 1251-8050.

Mouhovski, J.T.; Temelkov, K.A.; Vuchkov, N.K. & Sabotinov, N.V. (2009b). Simultaneous growth of high quality $Ca_{1-x}Sr_xF_2$ boules by optimized Bridgman-Stockbarger apparatus. Reliability of high-transmission measurements, *Bulgarian Chemical Communications,* Vol.41, No.3, 253–260, ISSN: 0324-1130.

Nassau, K. (1961). Application of the Czochralski Method to Divalent Metal Fluorides. *Journal of Applied Physics*, Vol.32, No.10, 1820–1825, ISSN: 0021-8979.

Popov P.A.; Chernenok E.V.; Fedorov P.P.; Kuznetsov S.V.; Konyushkin V.A. & Basiev T.T. (2006). Heat Conduction of Single Crystals of Heterovalence Solid Solutions of Ytterbium and Praseodymium Fluorides in Calcium Fluoride, *Kondensirovannye Sredy Mezhfazovyh Granitz*, No.4, 320–321 (in Russian), ISSM: 160-6-867X.

Popov, P.A.; Fedorov, P.P.; Konyushkin, V.A.; Nakladov, A.N.; Kuznetsov, S.V.; Osiko, V.V. & Basiev T.T. (2008). Thermal Conductivity of Single Crystals of $Sr_{1-x}Yb_xF_{2+x}$ Solid Solution. *Doklady Physics*, Vol. 53, No. 8, 413–415 (in Russian), ISSN PRINT: 1028-3358. ISSN ONLINE: 1562-6903. DOI: 10.1134/S1028335808080016

Popov, P.A.; Fedorov, P.P.; Kuznetsov, S.V.; Konyushkin, V.A.; Osiko, V.V. & Basiev, T.T. (2008). Thermal Conductivity of Single Crystals of $Ca_{1-x}Yb_xF_{2+x}$ Solid Solutions, *Doklady Physics*, Vol. 53, No. 4, 198–200 (in Russian), ISSN PRINT: 1028-3358. ISSN ONLINE: 1562-6903. DOI: 10.1134/S102833580804006X

Popov, P.A.; Fedorov, P.P.; Kuznetsov, S.V.; Konyushkin, V.A.; Osiko, V.V. & Basiev, T.T. (2008). Thermal Conductivity of Single Crystals of $Ba_{1-x}Yb_xF_{2+x}$ Solid Solution. *Doklady Physics*, Vol. 53, No. 7, 353–355 (in Russian), ISSN PRINT: 1028-3358. ISSN ONLINE: 1562-6903. DOI: 10.1134/S1028335808070045

Sekerka, R.F. (1965). A stability function for explicit evaluation of the Mullins-Sekerka interface stability criterion. *Journal of Applied Physics*, Vol.36, No.1, 264–268, ISSN (printed): 0021-8979, ISSN (electronic): 1089-7550.

Sekerka, R.F. (1968). Morphological Stability, *Journal of Crystal Growth*, Vol.3/4, 71–81, ISSN: 0022-0248.

Sobolev, B.P. & Fedorov, P.P. (1978). Phase Diagrams of the CaF_2-(Y, Ln)F_3 Systems. I. Experimental. *Journal of the Less-common Metals*, Vol.60, 33–46, ISSN: 0022-5088.

Sobolev, B.P.; Golubev, A.M. & Herrero, P. (2003). Fluorite $M_{1-x}R_xF_{2+x}$ phases (*M* = Ca, Sr, Ba; *R* = Rare Earth Elements) as nanostructured materials. (2003). *Crystallography Reports*, Vol.48, No.1, 141–161, ISSN PRINT: 1063-7745.

Sorokin, N.I.; Buchinskaya, I.I.; Fedorov, P.P. & Sobolev, B.P. (2008). Electrical conductivity of a CaF_2-BaF_2 nanocomposite, *Inorganic materials*, Vol.44, No.2, 189–192, ISSN: 0020-1685.

Tiller W.A.; Jackson, K.A.; Rutter, J.W. & Chalmers. B. (1953). The redistribution of solute atoms during the solidification of metals. *Acta Metallurgica*, Vol.1, 428–437, ISSN: 0001-6160.

Turkina, T.M.; Fedorov, P.P. & Sobolev, B.P. (1986). Stability of the flat crystallization front during growing from melt of mono-crystals of $M_{1-x}R_xF_{2+x}$ solid solutions (where M = Ca, Sr, Ba; R – rare earth elements). *Kristallografiya*, Vol.31, No.1, 146–152 (in Russian), ISSN PRINT: 0023-4761.

Van-der-Vaal's, I.D. & Konstamm, F. (1936). Course in thermostatic, Vol.1, ONTI, Moskwa (in Russian).

Weller, P.F.; Axe, J.D. & Pettit, G.D. (1965). Chemical and Optical Studies of Samarium Doped CaF_2 Type Single Crystals, *Journal of Electrochemical Society*, Vol.112, 74–77, ISSN: 1945-7111 online; ISSN: 0013-4651 print.

Wrubel, G.P.; Hubbard, B.E.; Agladge, N.I. et al. (2006). Glasslike Two-Level Systems in Minimally Disordered Mixed Crystals, *Physical Review Letters*, 2006, Vol.96, 235503-235507, ISSN: 0031-9007.

Yushkin, N.P.; Volkova, N.V. & Markova, G.A. (1983). *Optical fluorite*, Nauka, Moskva (in Russian).

Zhigarnovskii, B.M. & Ippolitov, E.G. (1969). Phase Diagram of the CaF_2–BaF_2 System, *Izvestii Akademii Nauk SSSR, Neorganicheskie Materialy*, Vol.5, No.9, 1558–1562 (in Russian), ISSN: 0002-337X.
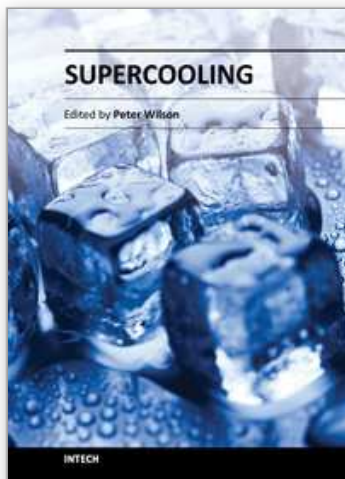
Supercooling

Edited by Prof. Peter Wilson

Supercooled liquids are found in the atmosphere, in cold hardy organisms, in metallurgy, and in many industrial systems today. Stabilizing the metastable, supercooled state, or encouraging the associated process of nucleation have both been the subject of scientific interest for several hundred years. This book is an invaluable starting point for researchers interested in the supercooling of water and aqueous solutions in biology and industry. The book also deals with modeling and the formation subsequent dendritic growth of supercooled solutions, as well as glass transitions and interface stability.

How to reference

In order to correctly reference this scholarly work, feel free to copy and paste the following:

INTECH
open science | open minds